Neurobiology of Disease

Na–K–Cl Cotransporter-Mediated Intracellular Na^+ Accumulation Affects Ca^{2+} Signaling in Astrocytes in an *In Vitro* Ischemic Model

Brett Lenart,[1] Douglas B. Kintner,[1] Gary E. Shull,[3] and Dandan Sun[1,2]

Departments of [1]Neurosurgery and [2]Physiology, University of Wisconsin Medical School, Madison, Wisconsin 53792, and [3]Department of Molecular Genetics, Biochemistry, and Microbiology, University of Cincinnati, Cincinnati, Ohio 45267

Na–K–Cl cotransporter isoform 1 (NKCC1) plays an important role in maintenance of intracellular Na^+, K^+, and Cl^- levels in astrocytes. We propose that NKCC1 may contribute to perturbations of ionic homeostasis in astrocytes under ischemic conditions. After 3–8 hr of oxygen and glucose deprivation (OGD), NKCC1-mediated ^{86}Rb influx was significantly increased in astrocytes from NKCC1 wild-type ($NKCC1^{+/+}$) and heterozygous mutant ($NKCC1^{+/-}$) mice. Phosphorylated NKCC1 protein was increased in $NKCC1^{+/+}$ astrocytes at 2 hr of OGD. Two hours of OGD and 1 hr of reoxygenation (OGD/REOX) triggered an ~3.6-fold increase in intracellular Na^+ concentration ($[Na^+]_i$) in $NKCC1^{+/+}$ astrocytes. Inhibition of NKCC1 activity by bumetanide or ablation of the NKCC1 gene significantly attenuated the rise in $[Na^+]_i$. Moreover, $NKCC1^{+/+}$ astrocytes swelled by 10–30% during 20–60 min of OGD. Either genetic ablation of NKCC1 or inhibition of NKCC1 by bumetanide-attenuated OGD-mediated swelling. An NKCC1-mediated increase in $[Na^+]_i$ may subsequently affect Ca^{2+} signaling through the Na^+/Ca^{2+} exchanger (NCX). A rise in $[Ca^{2+}]_i$ was detected after OGD/REOX in the presence of a sarcoplasmic-endoplasmic reticulum (ER) Ca^{2+}-ATPase inhibitor thapsigargin. Moreover, OGD/REOX led to a significant increase in Ca^{2+} release from ER Ca^{2+} stores. Furthermore, KB-R7943 (2-[2-[4(4-nitrobenzyloxy)phenyl]ethyl]isothiourea mesylate), an inhibitor of reverse-mode operation of NCX, abolished the OGD/REOX-induced enhancement in filling of ER Ca^{2+} stores. OGD/REOX-mediated Ca^{2+} accumulation in ER Ca^{2+} stores was absent when NKCC1 activity was ablated or pharmacologically inhibited. These findings imply that stimulation of NKCC1 activity leads to Na^+ accumulation after OGD/REOX and that subsequent reverse-mode operation of NCX contributes to increased Ca^{2+} accumulation by intracellular Ca^{2+} stores.

Key words: **cortical astrocytes; ischemia; intracellular Ca^{2+}; astrocyte swelling; Na^+ influx; Na^+/Ca^{2+} exchange**

Introduction

Na–K–Cl cotransporter isoform 1 (NKCC1) belongs to the cation-dependent Cl^- transporter family and transports Na^+, K^+, and Cl^- into cells under physiological conditions (Russell, 2000). NKCC1 is expressed in rat cortical astrocytes (Yan et al., 2001), oligodendrocytes (Hoppe and Kettenmann, 1989; Wang et al., 2003), and Schwann cells (Alvarez-Leefmans, 2001). Functions of NKCC1 in these cells include K^+ and Na^+ uptake (Su et al., 2000, 2002b) and accumulation of Cl^- above its electrochemical equilibrium (Hoppe and Kettenmann, 1989; Wang et al., 2003). In recent studies, we found that NKCC1 contributes to K^+ uptake, swelling, and swelling-induced glutamate release in astrocytes in the presence of high extracellular K^+ (Su et al., 2002a,b).

Received March 10, 2004; revised Aug. 26, 2004; accepted Aug. 28, 2004.

This work was supported in part by National Institutes of Health (NIH) Grant R01NS38118, National Science Foundation CAREER Award IBN9981826 (D.S.), and NIH Grant R01HL61974 (G.E.S.). We thank Dr. Robert Haworth for helpful discussion.

Correspondence should be addressed to Dr. Dandan Sun, Department of Neurological Surgery, University of Wisconsin Medical School, H4/332 Clinical Sciences Center, 600 Highland Avenue, Madison, WI 53792. E-mail: sun@neurosurg.wisc.edu.

DOI:10.1523/JNEUROSCI.2569-04.2004

 0270-6474/04/249585-13$15.00/0

Disruption of Na^+ and Ca^{2+} homeostasis plays an important role in ischemic cell damage (Siesjö, 1992). A steep inwardly directed Na^+ gradient is essential for glial functions, such as glutamate reuptake and regulation of intracellular ion concentrations by other secondary ion transporters (Walz, 1989; Longuemare et al., 1999). Breakdown of the Na^+ gradient is one of the key elements in promoting cellular damage in astrocytes during energy failure (Longuemare et al., 1999). An increase in intracellular Na^+ concentration ($[Na^+]_i$) was found in rat spinal cord astrocytes (Rose et al., 1998), rat cortical astrocytes (Longuemare et al., 1999), and mouse cortical astrocytes (Silver et al., 1997) when these cells were exposed to glucose deprivation, NaN_3-mediated chemical hypoxia, and simulated ischemia, respectively. Mechanisms of the rise in $[Na^+]_i$ under reduced energy production conditions are not well understood. Inhibition of Na^+/K^+–ATPase activity via limited energy production results in Na^+ accumulation (Silver et al., 1997). However, blocking voltage-gated Na^+ channels had no effect on the rise of $[Na^+]_i$ in rat spinal astrocytes during chemical hypoxia (Rose et al., 1998). It remains to be clarified which other Na^+ entry pathways contribute to Na^+ accumulation in astrocytes under energy deprivation.

Reduction in the Na^+ gradient affects Ca^{2+} homeostasis in cells. Elevation of $[Na^+]_i$ increases intracellular Ca^{2+} via

reverse-mode operation of the Na^+/Ca^{2+} exchanger (NCX) in neurons and causes irreversible injury during anoxia and ischemia (Li et al., 2000). An increase in intracellular Ca^{2+} via the reverse-mode operation of NCX occurs in rat astrocytes when $[Na^+]_i$ was raised by inhibition of Na^+/K^+–ATPase activity or activation of AMPA channels (Goldman et al., 1994; Smith et al., 2000). However, it is unknown whether accumulation of intracellular Na^+ during anoxia and ischemia can trigger Ca^{2+} entry in astrocytes via the reverse-mode operation of NCX.

In the present study, we examined Na^+ entry mediated by NKCC1 after 2 hr of oxygen and glucose deprivation and 1 hr of reoxygenation (OGD/REOX) and the subsequent effects on Ca^{2+} signaling in mouse cortical astrocytes. We found that NKCC1 activity contributes to intracellular Na^+ overload and Ca^{2+} accumulation in intracellular Ca^{2+} stores. The latter is in part a result of the reverse-mode operation of NCX.

Materials and Methods

Materials. Eagle's modified essential medium and HBSS were from Mediatech Cellgro (Herndon, VA). Fetal bovine serum was obtained from HyClone (Logan, UT). Collagen type I was from Collaborative Biomedical Products (Bedford, MA). Nigericin, bradykinin, thapsigargin, carbonyl cyanide *p*-trifluoromethoxyphenylhydrazone (FCCP), oligomycin, rotenone, and β-actin monoclonal antibody were purchased from Sigma (St. Louis, MO). GFAP monoclonal antibody was purchased from Sternberger Monoclonals (Lutherville, MD). Sodium binding benzofuran isophthalate AM (SBFI AM), fluorescein–methylene–iminodiacetate AM (calcein AM), 4-bromo A-23187 (calcimycin/5-(methylamino)-2[(2*R*,3*R*,6*S*,8*S*,9*R*,11*R*)-3,9,11-trimethyl-8-[(1*S*-1-methyl-2-oxo-2-(1H)-pryrrol-2-yl)-ethyl]-1,7-dioxaspiro[5.5]undec-2-yl]methyl-4-benzoxazolecarboxylic acid), and fura-2 AM were from Molecular Probes (Eugene, OR). Rubidium-86 was purchased from PerkinElmer Life Sciences (Emeryville, CA). KB-R7943 (2-[2-[4(4-nitrobenzyloxy) phenyl]ethyl]isothiourea mesylate) was from Tocris (Ellisville, MO). 2-Aminoethoxydiphenylborate (2-APB) was from EMC Biosciences (San Diego, CA). R5 polyclonal antibody was characterized previously (Flemmer et al., 2002) and was a kind gift from Dr. Biff Forbush (Yale University, New Haven, CT).

Animals and genotype analysis. NKCC1 homozygous mutant and wild-type mice were obtained by breeding gene-targeted NKCC1 heterozygous mutant mice, and genotypes were determined by PCR analysis of DNA from tail biopsies as described previously (Flagella et al., 1999; Su et al., 2002b).

Primary culture of mouse cortical astrocytes. Dissociated cortical astrocyte cultures were established as described previously (Su et al., 2002b). Cerebral cortices were removed from 1-d-old $NKCC1^{+/+}$, $NKCC1^{+/-}$, or $NKCC1^{-/-}$ mice. The cortices were incubated in a trypsin solution (0.25 mg/ml HBSS) for 25 min at 37°C. The dissociated cells were rinsed and resuspended in Eagle's minimum essential medium (EMEM) containing 10% fetal bovine serum. Viable cells (1×10^4 cells per well) were plated in 24-well plates or on glass coverslips in 6-well plates and coated with collagen type-1. Cultures were maintained in a 5% CO_2 atmosphere at 37°C and refed every 3 d throughout the study. To obtain morphologically differentiated astrocytes, confluent cultures [10 d in culture, 10 d *in vitro* (DIV)] were treated with EMEM containing 0.25 mM dibutyryl cAMP (dBcAMP) to induce differentiation. dBcAMP has been widely used to mimic neuronal influences on astrocyte differentiation (Swanson et al., 1997). Experiments were routinely performed in cultures 10–21 DIV.

OGD model. $NKCC1^{+/+}$, $NKCC1^{+/-}$, or $NKCC1^{-/-}$ astrocyte cultures in 24-well plates were rinsed twice with an isotonic OGD solution, pH 7.4, containing as follows (in mM): 0 glucose, 26 $NaHCO_3$, 120 NaCl, 5.36 KCl, 0.33 Na_2HPO_4, 0.44 KH_2PO4, 1.27 $CaCl_2$, and 0.81 $MgSO_4$. Cells were incubated in 0.5 ml of the OGD solution in a hypoxic incubator (model 3130; Forma Scientific, Marietta, OH) containing 94% N_2, 1% O_2, and 5% CO_2. During the initial 30 min of OGD, the plates were placed on an orbital shaker (model M48215; Thermolyne, Dubuque, IA) to facilitate equilibration of the hypoxic gases. The OGD incubation was 2 or 8 hr. Normoxic control cells were incubated in 5% CO_2 and atmospheric air in an isotonic control solution for 2 or 8 hr. The solutions used for normoxic control and reoxygenation contained 5.5 mM glucose, and the rest of the components in the buffer were identical to the OGD solution. Cells grown on coverslips in six-well plates were treated similarly as described above, except the solution volumes were 1.0 ml.

K^+ influx determination. NKCC1 activity was measured as bumetanide-sensitive K^+ influx, using ^{86}Rb as a tracer for K^+ (Sun and Murali, 1999). Briefly, cultured astrocytes were equilibrated for 3 min at 37°C with an isotonic HEPES-buffered minimum essential medium (MEM; 312 mOsm). The concentrations of components in HEPES–MEM were described previously (Schomberg et al., 2001). Cells were preincubated for 5 min in HEPES–MEM containing either 10 μM bumetanide and or 1 mM ouabain. For assay of NKCC1 or Na^+/K^+–ATPase activity, cells were exposed to 1 μCi/ml ^{86}Rb in HEPES–MEM for 3 min in the presence of 10 μM bumetanide and/or 1 mM ouabain. Radioactivity of cells extracted in 1% SDS was analyzed by liquid scintillation counting (1900CA; Packard, Downers Grove, IL). The ^{86}Rb influx rate was then calculated as the slope of ^{86}Rb uptake over time and expressed as nanomoles of ^{86}Rb per milligram of protein per minute. ^{86}Rb influx is linear over 7 min (Schomberg et al., 2001). Quadruplet determinations were obtained in each experiment throughout the study, and protein content was determined using the BCA method (Pierce, Rockford, IL).

Immunoprecipitation, gel electrophoresis, and immunoblotting. After normoxic or OGD treatments, cortical astrocytes were washed with ice-cold PBS, pH 7.4, containing phosphatase inhibitors (100 mM NaF, 10 mM $Na_4P_2O_7$, 2 mM $NaVO_3$, and 0.2 μM microcystin) and protease inhibitors as described previously (Sun and Murali, 1999). Immunoprecipitation was performed as described previously (Schomberg et al., 2003). Cells were lysed and centrifuged at 320 × *g* for 5 min. The supernatant fraction was collected and centrifuged at 45,000 rpm (SW 55 rotor; Beckman, Fullerton, CA) at 4°C for 30 min. The membrane pellet was resuspended in 0.25 ml of PBS–1% SDS for 30 min at room temperature, and the protein content of the membrane suspension was determined. Two hundred fifty micrograms of membrane protein from each sample were incubated in 0.875 ml of PBS–2% 3-[(3-cholamidopropyl)dimethylammonio]-1-propanesulfonate (CHAPS) at 4°C for 30 min. Samples were centrifuged at 320 × *g* for 5 min, and the supernatant was collected. Fifteen microliters of a T4 monoclonal antibody (T4 ascites; Departmental Studies Hybridoma Bank, Iowa City, IA) (Lytle et al., 1995) were then added, and samples were rotated on a shaker overnight at 4°C. T4 monoclonal antibody recognizes NKCC1, NKCC2, and spliced isoforms of NKCC1. For immunoprecipitation, 40 μl of a 30% slurry of protein G–Sepharose was added, and the samples were rotated for 2 hr at 4°C. The samples were washed four times with PBS–2% CHAPS and one time with PBS. The samples were denatured in SDS reducing buffer (Bio-Rad, Hercules, CA) and heated at 55°C for 30 min before gel electrophoresis.

The samples and prestained molecular mass markers (Bio-Rad) were then electrophoretically separated on a 6% acrylamide gel (Laemmli, 1970), and the resolved proteins were electrophoretically transferred to a polyvinylidene difluoride membrane (Sun and Murali, 1999). The blots were incubated in 7.5% nonfat dry milk in Tris-buffered saline (TBS) for 2 hr and then incubated for 3 hr with a primary polyclonal antibody (R5) against a diphosphopeptide containing T^{184} and T^{189} of shark NKCC1 (NKCC-p; 1:2000) (Flemmer et al., 2002). The blots were rinsed with TBS and incubated with horseradish peroxidase-conjugated secondary IgG for 1 hr (1:3000). Bound secondary antibody was visualized using the enhanced chemiluminescence (ECL) assay (Amersham Biosciences, Piscataway, NJ).

To confirm that each sample contained a similar amount of nonphosphorylated NKCC1 protein before immunoprecipitation, 30 μg of membrane protein from each sample was used directly for immunoblotting with the T4 antibody (1:3000). Expression of β-actin was monitored as an internal control with a monoclonal antibody (1:200).

After the ECL reaction, NKCC1 protein bands on the film were scanned using a Hewlett-Packard ScanJet (4c/T) scanner. The intensity of each band was measured by UN-SCAN-IT gel software (Silk Scientific, Orem, UT). We determined previously that the T4 signal is proportional to protein with loads between 15 and 45 μg (Yan et al., 2001).

Intracellular Na^+ measurement. $[Na^+]_i$ was measured in cultured as-

trocytes grown on coverslips with the fluorescent dye SBFI AM as described previously (Su et al., 2002b). At the end of 2 hr of OGD, astrocytes were loaded with 10 μM SBFI AM at room temperature in HEPES–MEM containing 0.05% pluronic acid for 45 min. The coverslips were then placed in an open-bath imaging chamber (model RC24; Warner Instruments, Hamden, CT) containing HEPES–MEM at ambient temperature. Astrocytes were excited every 10 sec at 345 and 385 nm, and the emission fluorescences at 510 nm were recorded with a Nikon (Melville, NY) TE 300 inverted epifluorescence microscope and a 40× Super Fluor oil immersion objective lens. Images were collected at 60 min REOX; 340/380 ratios were recorded for 5 min; and absolute $[Na^+]_i$ was determined for each cell as described previously (Su et al., 2002b).

For a more severe ischemic insult, a hypoxic, acidic, ion-shifted Ringer's (HAIR) buffer was used. Astrocytes grown on coverslips were loaded with 10 μM SBFI AM in HEPES–MEM containing 0.05% pluronic acid for 60 min at 37°C. The coverslips were then placed in an imaging chamber and continuously superfused with HEPES–MEM at 37°C to collect baseline data. After 2 min of baseline perfusion, the cells were superfused with HAIR buffer for 3 min. For reoxygenation, cells were perfused with normoxic HEPES–MEM for 6 min. For the bumetanide treatment study, 5 μM bumetanide was present in loading and all of the subsequent perfusion buffers. The ionic composition of HAIR was as follows (in mM): 34 NaCl, 13 $NaHCO_3$, 3 Na-gluconate, 65 K-gluconate, 38 NMDG-Cl, 1 NaH_2PO_4, 0.13 $CaCl_2$, 1.5 $MgSO_4$, and 0 glucose (Bondarenko and Chesler, 2001). HAIR buffer, pH 6.6, was sparged with 15% CO_2 and 85% N_2 for at least 1 hr before the experiment. An average O_2 of 1.9 ± 0.2% was determined at the entrance of the chamber using a flow-through oxygen electrode (model 16-730; Microelectrodes , Bedford, NH).

Intracellular ^{36}Cl measurement. Intracellular ^{36}Cl content was measured in astrocytes grown in 24-well plates. After OGD or normoxia, cells were preincubated at 37°C for 30 min in HEPES–MEM containing ^{36}Cl (0.4 μCi/ml), as described previously (Su et al., 2002a), in the presence or absence of 10 μM bumetanide. In our previous study, steady-state intracellular ^{36}Cl was reached by 10 min incubation and maintained for 60 min (Su et al., 2002a). Thus, a 30 min preincubation with ^{36}Cl was used in the current study. Intracellular ^{36}Cl content measurement was terminated by three washes with 1 ml of ice-cold washing buffer (Su et al., 2002a). Radioactivity of the cellular extract in 1% SDS was analyzed by liquid scintillation counting (1900CA; Packard). In each experiment, specific activities (counts per micromole per minute) of ^{36}Cl were determined for each assay condition and used to calculate intracellular Cl^- content (micromoles per milligram per protein). Protein content was measured in each sample using the BCA method (Pierce).

Intracellular Ca^{2+} measurement. To determine changes in $[Ca^{2+}]_i$ at 1 hr of REOX after 2 hr of OGD, astrocytes were incubated with 5 μM fura-2 AM at the end of 2 hr of OGD for 45 min (at room temperature). For experiments in determination of $[Ca^{2+}]_i$ at the end of 2 hr of OGD, the astrocytes were incubated with 5 μM fura-2 AM during the 2 hr of OGD treatment. Our pilot study indicated that a short period of OGD (2 hr) did not significantly decrease the energy level in astrocytes and that the fluorescence dye loading during OGD was sufficient.

Astrocytes on coverslips were then placed in the open-bath imaging chamber containing HEPES–MEM at ambient temperature. Using a Nikon TE 300 inverted epifluorescence microscope and a 40× Super Fluor oil immersion objective lens, astrocytes were excited every 10 sec at 345 and 385 nm, and the emission fluorescence at 510 nm was recorded. Images were collected and analyzed with the MetaFluor image-processing software. At the end of each experiment, the cells were exposed to 1 mM $MnCl_2$ in Ca^{2+}-free HEPES–MEM. The Ca^{2+}-insensitive fluorescence was subtracted from each wavelength before calculations (Haworth and Redon, 1998). The $MnCl_2$-corrected 345/385 emission ratios were converted to concentration using the Grynkiewicz equation (Grynkiewicz et al., 1985) as follows:

$$[Ca^{2+}] = K_d \times \left(\frac{R - R_{min}}{R_{max} - R}\right) \times \beta,$$

where R is the experimental 345/385 ratio; R_{min} is the ratio in HEPES–MEM without Ca^{2+} and containing 1 mM EGTA and 1 μM 4-bromo A-23187; R_{max} is the ratio in HEPES–MEM with 10 mM Ca^{2+} and 1 μM 4-bromo A-23187 plus 4 μM rotenone and 2 μM FCCP to inhibit active Ca^{2+} transport by mitochondria; β is the ratio of the 385 nm fluorescence intensities determined at R_{min} and R_{max}; and K_d is the *in vivo* dissociation constant for the dye and was assumed to be 370 nM (Petr and Wurster, 1997).

Bradykinin-induced Ca^{2+} release measurement. Bradykinin-induced Ca^{2+} release from intracellular stores was assessed by exposing astrocytes to 1 μM bradykinin in Ca^{2+}-free HEPES–MEM (1 mM EGTA) to prevent entry of extracellular Ca^{2+}. Peak Ca^{2+} release was measured after application of bradykinin. Within 5 min, $[Ca^{2+}]_i$ returned to basal levels. In some cells, spontaneous Ca^{2+} signaling was present before application of bradykinin, which prevented an accurate prebradykinin $[Ca^{2+}]_i$ baseline determination. In those cases, a Ca^{2+}-free baseline after 5 min of bradykinin exposure was considered to be the basal $[Ca^{2+}]_i$. After washout of bradykinin, cells were exposed to 1 μM thapsigargin to assess residual Ca^{2+} release from bradykinin-insensitive Ca^{2+} stores.

In some experiments, Ca^{2+} release from mitochondria was monitored after application of FCCP (10 μM) to collapse the mitochondria membrane potential and oligomycin (2.5 μg/ml) to block F_1F_0–ATP synthase. After a new baseline of $[Ca^{2+}]_i$ was established after this treatment, cells were exposed to 1 μM bradykinin in the presence of FCCP–oligomycin.

Measurement of reverse-mode operation of NCX. NKCC1$^{+/+}$ astrocytes grown on coverslips were incubated with 5 μM fura-2 AM, and cytosolic Ca^{2+} concentrations were measured as described above. The reverse-mode operation of NCX was induced by exposing cells to a Na^+- and Ca^{2+}-free buffer (1 min) followed by a Na^+-free buffer that contained Ca^{2+} (2 min). The effect of an NCX inhibitor, KB-R7943 (0–10 μM), on reverse-mode activity of NCX was investigated. Intracellular Ca^{2+} levels after induction of the reverse-mode NCX activity were measured, and the percentage of inhibition at given concentrations of KB-R7943 was calculated in each cell by comparing the $[Ca^{2+}]_i$ levels at 0 μM KB-R7943 with $[Ca^{2+}]_i$ levels in the presence of the particular concentration of KB-R7943.

Measurement of cell swelling. Relative cell volume changes were monitored during OGD on either NKCC1$^{+/+}$ or NKCC1$^{-/-}$ cells grown on coverslips. Coverslips were placed in a closed-bath imaging chamber (model RC20; Warner Instruments) and perfused continuously at 36°C. The chamber was connected via a manifold to two reservoirs. One contained HEPES–MEM, and the other contained HEPES–MEM lacking glucose and bubbled with 100% N_2 for OGD. Oxygen levels of the perfusate were monitored at the entrance of the chamber using a flow-through oxygen electrode. After 30 min of normoxic control perfusion, the chamber was switched to OGD. Oxygen levels reached 2–5% within 2 min and were then maintained at the same level for 60 min.

Relative cell volume changes during OGD were monitored using video-enhanced differential interference contrast (DIC) microscopy, as described in our previous study (Su et al., 2002b). A single astrocyte was visualized every 10 min using a 60× Plan Fluor DIC objective lens, and the images were recorded. The mean cross-sectional area (CSA) was calculated after tracing the perimeter of the cell body with MetaMorph image-processing software.

In addition, cell volume change in single cells was also confirmed by using calcein as a marker of intracellular water volume as described previously (Hamann et al., 2002). Briefly, astrocytes grown on coverslips were placed in a closed-bath imaging chamber and incubated with 2.5 μM calcein AM. Calcein fluorescence in cells was monitored using a 40× Super Fluor oil immersion objective and an FITC filter set [excitation (Ex), 480 nm; emission (Em), 535 nm] (Chroma Technology, Rockingham, VT) until the fluorescence plateaued (~30 min). Images were collected every 60 sec for 10 min to determine baseline data. The chamber was then switched to OGD buffer for 60 min.

The fluorescence signals were corrected for baseline drift by fitting a single exponential curve to the 10 min control period. The relationship between baseline-corrected calcein fluorescence and external osmolality was characterized by exposing the cells to salt-constant hyperosmotic and hypo-osmotic solutions for 1–2 min, during which time no regulatory volume decrease had yet been initiated (Su et al., 2002b). The osmolality of the buffers was adjusted as described before (Su et al., 2002b).

The standards were corrected for the relative background signal. This signal is the fraction of intracellular calcein fluorescence that is insensitive to changes in external osmolality (the *y*-intercept of a plot of relative cell volume vs the reciprocal of the relative osmotic pressure) (Hamann et al., 2002). The standard fluorescence changes were plotted as a function of the reciprocal of the relative osmotic pressure, and the resulting calibration curve was applied to each experiment.

Measurement of intracellular ATP content. Intracellular ATP content was measured using a luminescence ATP detection assay (PerkinElmer Life Sciences). After 8 hr of OGD or 2 hr of OGD plus 1 hr of REOX, culture medium was removed, and 100 μl of fresh OGD or normoxic control buffer was added to each well. Fifty microliters of lysis solution were added, and plates were gently swirled for 5 min. Aliquots of cell lysates (diluted at 1:10) were added to 50 μl of substrate buffer. Luminescence was detected with an LMax II Luminometer (Molecular Devices, Sunnyvale, CA). In each experiment, ATP levels were determined using ATP standards run concurrently with samples. Protein content in cell lysates was determined in each sample using the BCA method (Pierce). Intracellular ATP content is expressed as nanomoles per milligram of protein.

Measurement of cell death. Cell viability was assessed by propidium iodide (PI) uptake and retention of calcein using a Nikon TE 300 inverted epifluorescence microscope. Cultured astrocytes were rinsed with HEPES–MEM buffer and incubated with 1 μg/ml calcein AM and 10 μg/ml PI in the same buffer at 37°C for 25 min. For cell counting, cells were rinsed and visualized using a Nikon 20× objective lens. Calcein fluorescence was visualized using FITC filters (Ex, 488 nm; Em, 515 nm), and PI fluorescence was visualized with Texas Red filters (Ex, 536 nm; Em, 645 nm). Images were collected in a blind manner, and a total of 1000 cells per condition were counted using MetaMorph image-processing software (Universal Imaging, Downingtown, PA). Cell mortality was expressed as the ratio of PI-positive cells to the sum of calcein- and PI-positive cells.

Statistics. Throughout the study, *n* values represented numbers of cultures used in each experiment. Routinely, parameters were measured in ~20 cells on a coverslip from each culture. Statistical significance was determined by ANOVA (Bonferroni–Dunn) at a confidence of 95% ($p < 0.05$).

Results

Expression of NKCC1 protein in astrocytes

To determine relative NKCC1 protein expression in astrocytes of three genotypes, immunoblotting was performed with lysate samples of astrocytes from NKCC1$^{+/+}$, NKCC1$^{+/-}$, and NKCC1$^{-/-}$ mice (Fig. 1). Densitometric optical intensity was performed on immunoblots. NKCC1$^{+/+}$ astrocytes expressed abundant NKCC1 protein, and ~30% less NKCC1 protein was detected in NKCC1$^{+/-}$ astrocytes. No NKCC1 protein was found in NKCC1$^{-/-}$ astrocytes.

NKCC1 activity is increased after OGD

NKCC1 activity was measured using ^{86}Rb as a tracer for K^+ after 3–8 hr of OGD. Bumetanide-sensitive ^{86}Rb influx in NKCC1$^{+/+}$ astrocytes was increased from a control level of 17.3 ± 3.1 to 33.1 ± 2.8 nmol/mg of protein after 3 hr of OGD ($p < 0.05$). Bumetanide-sensitive ^{86}Rb influx remained elevated after 8 hr of OGD (23.1 ± 2.8 vs 13.7 ± 2.4 nmol/mg of protein) (Fig. 2*A*). Similarly, in NKCC1$^{+/-}$ astrocytes, 8 hr of OGD also led to an increase in bumetanide-sensitive ^{86}Rb influx (Fig. 2*A*). The bumetanide-sensitive ^{86}Rb influx was negligible in NKCC1$^{-/-}$ astrocytes (Su et al., 2002b). Therefore, no measurements were performed in NKCC1$^{-/-}$ astrocytes.

To determine whether Na^+/K^+–ATPase-mediated K^+ influx was altered after OGD, ouabain-sensitive ^{86}Rb influx was measured. After 8 hr of OGD, total ^{86}Rb influx was reduced from 93.7 ± 8.8 to 72.9 ± 7.2 nmol/mg of protein (Fig. 2*B*) ($p < 0.05$). Ouabain-sensitive ^{86}Rb influx was reduced from a control level of 50.7 ± 6.9 to 32.6 ± 4.5 nmol/mg of protein ($p < 0.05$). Moreover, ^{86}Rb influx that was insensitive to both ouabain and bumetanide was reduced from 36.8 ± 10.0 to 23.2 ± 4.9 nmol/mg of protein. Thus, only NKCC1-mediated ^{86}Rb influx in astrocytes was elevated after OGD, whereas ^{86}Rb influx from Na^+/K^+–ATPase activity, other transporters, or channels was decreased.

We then investigated whether stimulation of NKCC1 in astrocytes after OGD can be detected by measuring changes in phosphorylated NKCC1. The R5 polyclonal antibody against a diphosphopeptide containing T^{184} and T^{189} of NKCC1 (Darman and Forbush, 2002) was used to probe the phosphorylation state of NKCC1. T^{184}, T^{189}, and T^{202} of the N terminus represent a conserved phosphoregulatory domain of NKCC1 (Darman and Forbush, 2002). Total NKCC1 protein was immunoprecipitated with T4 monoclonal antibody. Subsequently, immunoblots were probed with the R5 antibody. After 2 hr of OGD, phosphorylated NKCC1 protein (NKCC1-p) in NKCC1$^{+/+}$ astrocytes was increased compared with controls (Fig. 3*A*). OGD increased levels of NKCC1-p by ~300% (299 ± 82%; $n = 3$; $p < 0.05$). To determine whether there was an upregulation of total NKCC1 protein, the same protein samples were probed with T4 antibody without immunoprecipitation (Fig. 3*B*). NKCC1 expression was similar in control and OGD-treated cells. In the same blot, no significant changes were observed in expression of β-actin. Together, OGD stimulates NKCC1 phosphorylation in NKCC1$^{+/+}$ astrocytes, which is consistent with elevation of NKCC1 activity measured with ^{86}Rb influx.

Inhibition of NKCC1 activity attenuated Na^+ and Cl^- accumulation after OGD

We speculated that the increased activity of NKCC1 after OGD may lead to Na^+ accumulation in astrocytes. Because we observed a significant increase in NKCC1 phosphorylation after 2 hr of OGD, we determined whether this increase in NKCC1 ac-

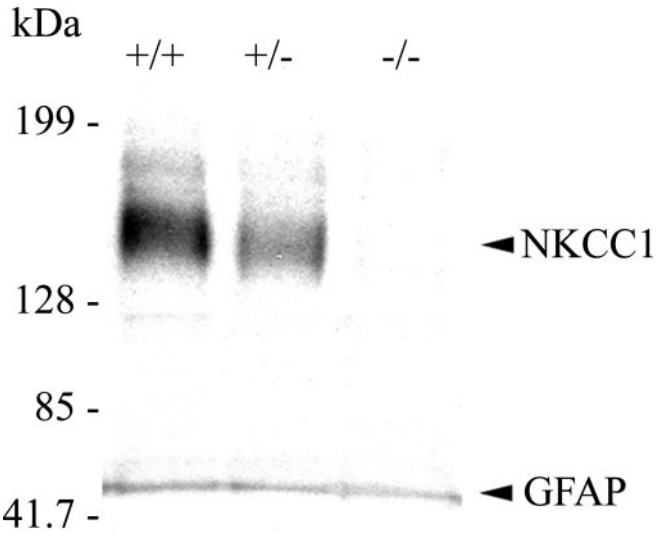

Figure 1. NKCC1 protein expression in astrocytes. NKCC1 protein expression in NKCC1$^{+/+}$, NKCC1$^{+/-}$, and NKCC1$^{-/-}$ cortical astrocytes was determined by immunoblotting. Thirty micrograms of protein per lane were separated by 6% SDS-PAGE, transferred to a nitrocellulose membrane, and probed with either T4 monoclonal antibody or GFAP monoclonal antibody. The immunoblots were visualized using ECL. This is a representative blot from one of five experiments. No signal was detected in the NKCC1$^{-/-}$ sample.

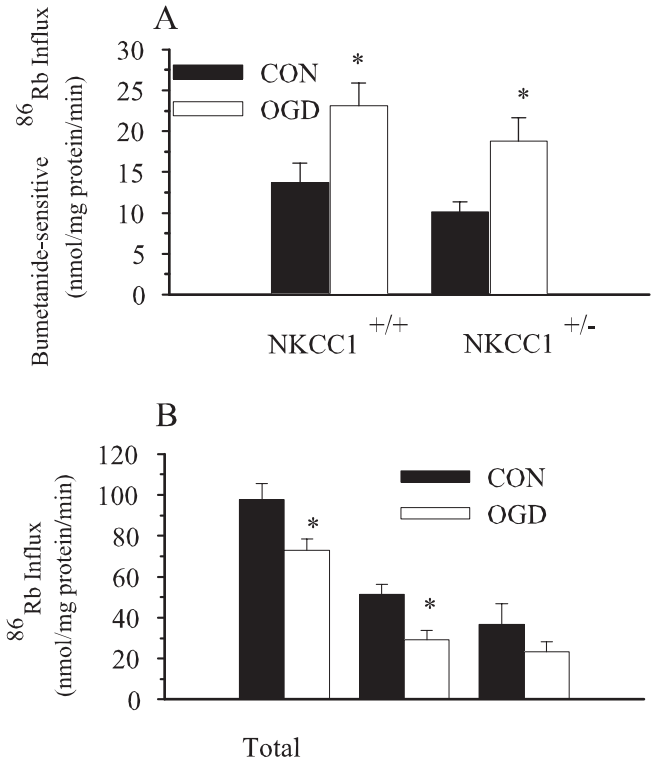

Figure 2. OGD stimulated NKCC1 activity. *A*, NKCC1 activity in astrocytes was assessed using ^{86}Rb as a tracer for K^+. After 8 hr of OGD, astrocytes were preincubated in HEPES–OGD buffer in the presence or absence of bumetanide (10 μM) for 5 min. ^{86}Rb influx was assayed subsequently for 3 min in identical HEPES–OGD buffer containing 1 μCi ^{86}Rb. Control (CON) measurements were performed in normoxic sister cultures. *B*, Astrocytes were preincubated in the presence or absence of bumetanide (10 μM) and/or ouabain (1 mM). ^{86}Rb influx was assayed as described above. Data are means ± SEM; $n = 5$; *$p < 0.05$ versus control.

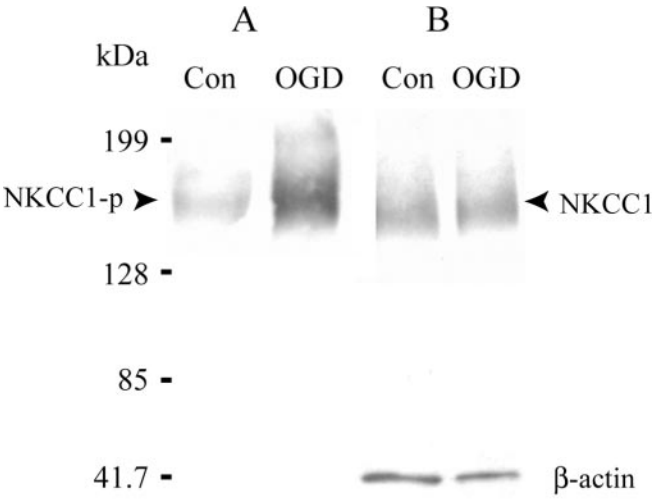

Figure 3. OGD caused increase in NKCC1 phosphorylation. *A*, After 2 hr of OGD, normoxic control (Con) and OGD astrocytes were rinsed with a buffer (see Materials and Methods), and 250 μg of membrane protein from each sample was used for immunoprecipitation with T4 monoclonal antibody. Samples were separated by 6% SDS-PAGE, transferred to a nitrocellulose membrane, and probed with R5 polyclonal antibody. *B*, Thirty micrograms of membrane protein from each sample were separated by 6% SDS-PAGE, transferred to a nitrocellulose membrane, and probed with T4 or β-actin antibodies.

tivity would cause intracellular Na^+ accumulation after 2 hr of OGD. As shown in Figure 4, the baseline $[Na^+]_i$ level in NKCC1 $^{+/+}$ astrocytes was 12.7 ± 0.6 mM after 3 hr normoxic incubation. After OGD/REOX, the $[Na^+]_i$ level in NKCC1 $^{+/+}$ astrocytes rose to 46.4 ± 5.0 mM ($p < 0.01$). Additionally, in NKCC1 $^{+/+}$ cells, inhibition of NKCC1 activity with 5 μM bumetanide reduced the rise in $[Na^+]_i$ (23.2 ± 0.9 mM; $p < 0.01$) (Fig. 4). Basal $[Na^+]_i$ in NKCC1 $^{-/-}$ cells was 12.6 ± 1.1 mM under control conditions, which was not different from that of NKCC1 $^{+/+}$ astrocytes. In contrast, in NKCC1 $^{-/-}$ astrocytes, the OGD/REOX-mediated rise in $[Na^+]_i$ was only 19.8 ± 0.6 mM ($p < 0.01$), significantly less than in NKCC1 $^{+/+}$ astrocytes (Fig. 4). Although the rise in $[Na^+]_i$ was attenuated in NKCC1 $^{-/-}$ cells after OGD/REOX, it remained significantly higher than in NKCC1 $^{-/-}$ cells under normoxic conditions. Together, blocking of astrocyte NKCC1 activity, either by genetic ablation or pharmacological inhibition, significantly reduced the accumulation of intracellular Na^+ after OGD and REOX.

We also measured intracellular ^{36}Cl content in NKCC1 $^{+/+}$ astrocytes after either 3 hr of normoxia or 2 hr of OGD and 1 hr of REOX. ^{36}Cl content was 0.27 ± 0.01 μg/mg of protein in the normoxia control group. It was increased to 0.31 ± 0.02 μg/mg of protein in the OGD/REOX-treated astrocytes ($p < 0.05$). Moreover, inhibition of NKCC1 activity with bumetanide (10 μM) abolished the increase in ^{36}Cl accumulation after OGD/REOX (0.22 ± 0.01 μg/mg of protein). Bumetanide had no significant affects on the basal level of ^{36}Cl content in astrocytes (0.26 ± 0.01 μg/mg of protein; $p > 0.05$). Thus, these data support the hypothesis that NKCC1 activation causes Na^+ and Cl^- accumulation in astrocytes after OGD and reoxygenation.

In the current OGD/REOX study, the ionic composition of the buffers is held constant. However, during *in vivo* ischemia, major ionic shifts occur in the extracellular space. Therefore, we investigated whether NKCC1 can contribute to Na^+ accumulation when astrocytes are exposed to a hypoxic buffer whose ionic composition was modified to mimic the interstitial milieu of the hypoxic brain (Bondarenko and Chesler, 2001). As shown in Table 1, $[Na^+]_i$ decreased to 70% of baseline in response to 3 min of HAIR treatment. This decrease can be attributable to either the experimental decrease in extracellular $[Na^+]$ ($[Na^+]_o$; 69 mM) or the stimulation of Na^+/K^+–ATPase by the elevated external K^+ (62 mM). In NKCC1 $^{+/+}$ astrocytes treated with 5 μM bumetanide, $[Na^+]_i$ decreased further to 38% of baseline during HAIR

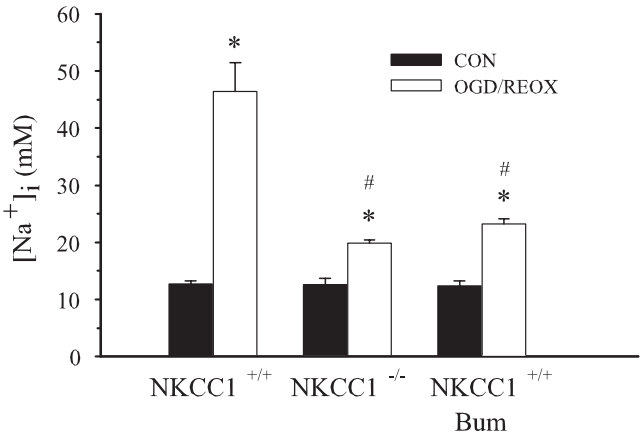

Figure 4. NKCC1 $^{-/-}$ astrocytes exhibited significantly less intracellular Na^+ accumulation after OGD. $[Na^+]_i$ was determined after OGD/REOX in NKCC1 $^{+/+}$ and NKCC1 $^{-/-}$ astrocytes. $[Na^+]_i$ in sister coverslips were determined after 3 hr of normoxic incubation. Data are means ± SEM; $n = 4$; *$p < 0.01$ versus control (CON); $^{\#}p < 0.01$ versus NKCC1 $^{+/+}$ OGD/REOX. Bum, Bumetanide.

Table 1. Changes of $[Na^+]_i$ in NKCC1$^{+/+}$ astrocytes after HAIR treatment

	$[Na^+]_i$ (mM)	
	Untreated	Bumetanide (5 μM)
Baseline	11.2 ± 0.3	11.5 ± 0.4
HAIR	7.8 ± 0.4	4.3 ± 0.5*
REOX	52.1 ± 2.9	29.3 ± 3.8*

$[Na^+]_i$ was determined after 3 min of HAIR exposure or 3 min of HAIR plus 6 min of REOX. Data are means ± SEM; $n = 4$; *$p < 0.01$ versus untreated.

exposure. When NKCC1$^{+/+}$ astrocytes were returned to HEPES–MEM, $[Na^+]_i$ quickly increased and plateaued to a level 4.6 times baseline within 6 min of REOX (Table 1). However, in bumetanide-treated NKCC1$^{+/+}$ astrocytes, the increase in $[Na^+]_i$ at 6 min of REOX was only 2.6 times baseline (Table 1). Thus, NKCC1 plays a similar role in Na^+ accumulation under the more pathophysiologically relevant HAIR model.

NKCC1$^{-/-}$ astrocytes exhibited less swelling after OGD

Increases in intracellular Na^+ and Cl^- will inevitably lead to cell swelling. We therefore investigated whether OGD would induce an increase in relative cross-sectional area (CSAr) in NKCC1$^{+/+}$ and NKCC1$^{-/-}$ astrocytes. We monitored swelling in NKCC1$^{+/+}$ and NKCC1$^{-/-}$ astroctyes with time. As shown in Figure 5*A*, after 20 min of OGD, CSAr in NKCC1$^{+/+}$ astroctyes increased by 10%, and after 60 min of OGD, it increased to ~30%. In contrast, changes in CSAr developed slowly in NKCC1$^{-/-}$ astroctyes. NKCC1$^{-/-}$ astroctyes exhibited only a 3% increase in CSAr at 20 min of OGD. After 1 hr of OGD, CSAr increased by 14% in NKCC1$^{-/-}$ astrocytes (Fig. 5*A*). These increases in CSAr are significantly less than those observed in NKCC1$^{+/+}$ astroctyes after 30, 40, 50, or 60 min of OGD (Fig. 5*A*).

We also examined whether pharmacological inhibition of NKCC1 activity blocked OGD-mediated swelling in NKCC1$^{+/+}$ astrocytes. After 1 hr of OGD, the CSAr of NKCC1$^{+/+}$ astrocytes increased by 47%. In the presence of bumetanide (5 μM), the increase in CSAr was 14% after 1 hr of OGD, similar to that of NKCC1$^{-/-}$ astrocytes (Fig. 5*B*).

To validate the DIC method as an accurate reflection of cell volume changes, we used a fluorescence-based calcein method. NKCC1$^{+/+}$ astrocytes were exposed to isotonic or hypotonic buffers, and cell swelling was monitored using both methods. As shown in Figure 5*C*, changes in relative cell volume correlated with the reciprocal of the relative osmotic pressure using either method (DIC, $r^2 = 0.98$; calcein, $r^2 = 0.99$). However, the slope of the DIC fit (0.64) was somewhat shallower than that of the calcein fit (0.88). This implies that the calcein method exhibits more ideal osmometric behavior and is likely to be more sensitive. The *y*-intercept corresponded to the fraction of the calcein that is insensitive to changes in external osmolarity.

Figure 5*D* shows that similar cell swelling was detected with the calcein method. During control perfusion, relative cell volume in NKCC1$^{+/+}$ astrocytes did not change (Fig. 5*D*). OGD caused a rapid increase in relative cell volume that reached levels similar to those measured with the DIC method. In NKCC1$^{+/+}$ cells treated with bumetanide, the increase in relative cell volume during OGD was greatly reduced (Fig. 5*D*). Together, the results with the calcein method confirm our conclusion that NKCC1 has an important role in OGD-mediated cell swelling.

OGD/REOX did not trigger significant changes in bulk $[Ca^{2+}]_i$ in astrocytes

Accumulation of intracellular Na^+ may increase $[Ca^{2+}]_i$ via reverse-mode operation of NCX in astrocytes (Smith et al., 2000).

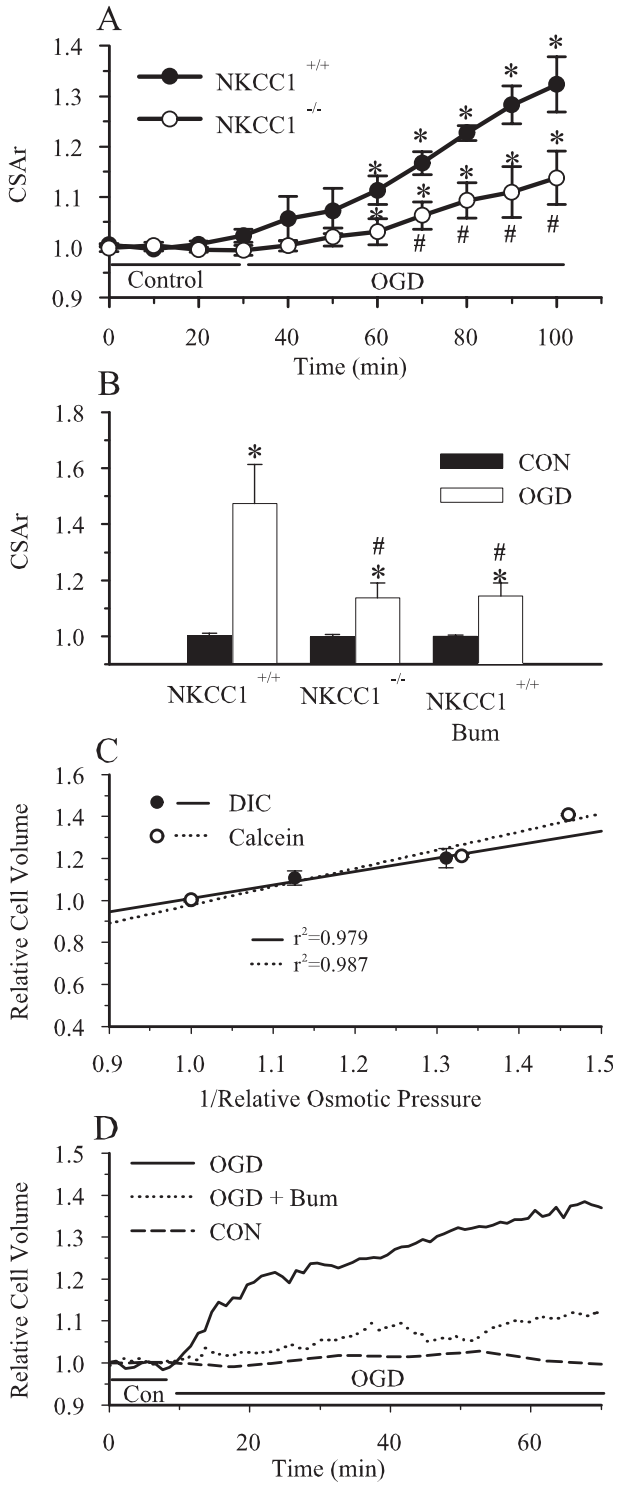

Figure 5. NKCC1$^{-/-}$ astrocytes showed less OGD-mediated swelling. *A*, Changes in CSAr of a single NKCC1$^{+/+}$ or NKCC1$^{-/-}$ astrocyte were assessed by DIC microscopy every 10 min during 30 min of control perfusion, followed by 60 min of OGD perfusion. Data are means ± SEM; $n = 3$; *$p <$ 0.01 versus control; #$p < 0.01$ versus NKCC1$^{+/+}$ OGD. *B*, Average changes in CSAr in single NKCC1$^{+/+}$ astrocytes during control perfusion or at the end of 60 min OGD. In bumetanide-treated cells, 5 μM bumetanide (Bum) was present during control and OGD perfusion. Data are means ± SEM; $n = 3$; *$p < 0.05$ versus control; #$p < 0.05$ versus NKCC1$^{+/+}$ OGD. *C*, A linear regression was fit to relative cell volume versus the reciprocal of the relative osmotic pressure using either the DIC or calcein method. DIC data were taken from Su et al. (2002b). Data are means ± SEM; $n = 4–6$. *D*, Average changes in the relative cell volume in NKCC1$^{+/+}$ astrocytes were determined with the calcein method during 10 min of control perfusion followed by 60 min of OGD. In the bumetanide experiments, cells were exposed to 5 μM bumetanide 30 min before OGD and during all of the subsequent perfusions. Data are means of 40 cells from two experiments in each group.

To test this hypothesis, we first measured $[Ca^{2+}]_i$ of NKCC1$^{+/+}$ and NKCC1$^{-/-}$ astrocytes under normoxic control conditions, 2 hr of OGD, and OGD/REOX. As shown in Figure 6*A*, similar basal $[Ca^{2+}]_i$ levels were found between NKCC1$^{+/+}$ and NKCC1$^{-/-}$ astrocytes under control conditions. In addition, neither OGD nor OGD/REOX caused a significant increase in $[Ca^{2+}]_i$ in NKCC1$^{+/+}$ or NKCC1$^{-/-}$ astrocytes.

Intracellular Ca^{2+} stores in astrocytes are a key component in astrocyte Ca^{2+} signaling (Smith et al., 2003). Therefore, it is possible that Ca^{2+} entry after OGD was buffered by an increase in Ca^{2+} uptake into intracellular Ca^{2+} stores. To test this possibility, we examined whether inhibition of Ca^{2+} uptake by an irreversible inhibitor of the endoplasmic reticulum (ER) Ca^{2+}–ATPase, thapsigargin, would reveal a rise in $[Ca^{2+}]_i$. As shown in Figure 6*B*, in the presence of 1.2 mM $[Ca^{2+}]_o$ and thapsigargin, a small elevation of $[Ca^{2+}]_i$ was detected in control NKCC1$^{+/+}$ astrocytes. Two hours of OGD and 1 hr of REOX triggered a twofold increase in $[Ca^{2+}]_i$ (Fig. 6*B*, inset). In contrast, inhibition of NKCC1 activity with bumetanide significantly attenuated the Ca^{2+} rise (Fig. 6*B*, inset).

We speculated that our OGD/REOX protocol causes a mild insult to astrocytes, which was reflected in the lack of change in bulk $[Ca^{2+}]_i$. To verify this, cell death assay was performed. Cell death in NKCC1$^{+/+}$ astrocytes after 2 hr of OGD or 2 hr of OGD plus 1 hr of REOX was negligible (Fig. 6*C*). Eight hours of OGD led to ~20% cell death ($p = 0.10$). To evaluate further the severity of the OGD insult, intracellular ATP content was measured after OGD/REOX and 8 hr of OGD. As shown in Figure 6*C* (inset), ATP content in control cells was 7.02 ± 0.90 nmol of ATP/mg of protein. After 2 hr of OGD, intracellular ATP was 4.71 ± 1.3 nmol of ATP/mg of protein but not significantly different from control levels. Eight hours of OGD caused a significant decrease in ATP levels (2.95 ± 0.60 nmol of ATP/mg of protein; $p < 0.05$).

Inhibition of NKCC1 activity reduced Ca^{2+} uptake mediated by intracellular Ca^{2+} stores

We investigated further Ca^{2+} release from Ca^{2+} stores in control and OGD/REOX-treated cells in the absence of extracellular Ca^{2+}. As shown in Figure 7*A*, 1.0 μM bradykinin triggered Ca^{2+} release from intracellular Ca^{2+} stores in NKCC1$^{+/+}$ astrocytes and raised $[Ca^{2+}]_i$ from a baseline of 70 ± 6 to 402 ± 38 nM under normoxic conditions. However, after 2 hr of OGD and 1 hr of REOX, bradykinin-induced Ca^{2+} release increased to 714 ± 34 nM ($p < 0.05$) (Fig. 7*A*). In NKCC1$^{-/-}$ astrocytes, bradykinin evoked a Ca^{2+} release under normoxic control conditions that was similar to that of NKCC1$^{+/+}$ cells (465 ± 50 nM) (Fig. 7*C*). In contrast, bradykinin-induced Ca^{2+} release in OGD-treated NKCC1$^{-/-}$ astrocytes (506 ± 89 nM) was not significantly different from that of control NKCC1$^{-/-}$ cells (Fig. 7*C*) but was significantly lower than in OGD-treated NKCC1$^{+/+}$ astrocytes. This suggests that OGD caused an increase in Ca^{2+} uptake by the intracellular Ca^{2+} stores in NKCC1$^{+/+}$ astrocytes but not in NKCC1$^{-/-}$ astrocytes.

As shown in Figure 7, *B* and *D*, a small fraction of Ca^{2+} release was insensitive to bradykinin but was triggered by thapsigargin. In contrast, when Ca^{2+} release was first evoked by 1.0 μM thapsigargin, bradykinin did not induce any additional Ca^{2+} release (data not shown). These results imply that astrocytes have both bradykinin-sensitive and -insensitive Ca^{2+} stores. Interestingly, NKCC1$^{-/-}$ astrocytes also exhibited significantly less Ca^{2+} release from bradykinin-insensitive Ca^{2+} stores than in NKCC1$^{+/+}$ astrocytes ($p < 0.05$) (Fig. 7*B*,*D*).

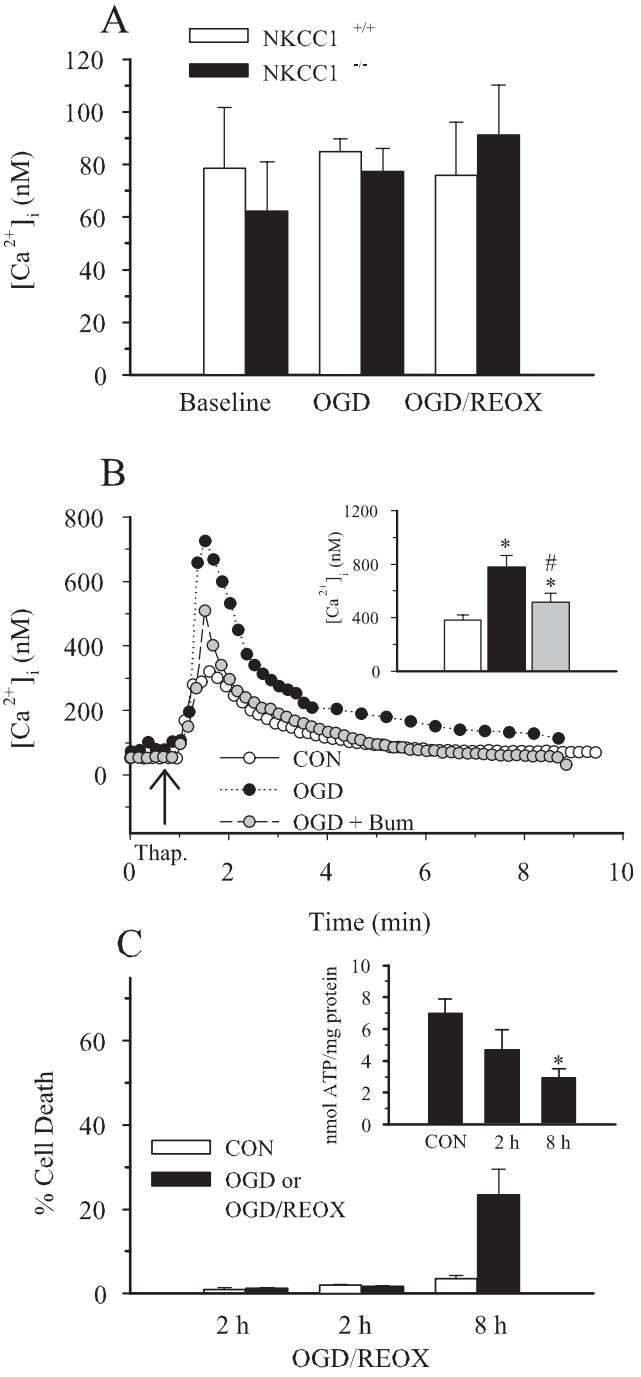

Figure 6. Effects of OGD/REOX on $[Ca^{2+}]_i$ and cell death. *A*, $[Ca^{2+}]_i$ was determined in NKCC1$^{+/+}$ or NKCC1$^{-/-}$ astrocytes immediately after 2 hr of OGD or OGD/REOX. Three hours of normoxic control experiments (baseline) were performed using NKCC1$^{+/+}$ and NKCC1$^{-/-}$ astrocytes. Data are means ± SEM; $n = 3$. *B*, Thapsigargin-induced Ca^{2+} release was determined under normal $[Ca^{2+}]_o$ conditions (1.2 mM) in NKCC1$^{+/+}$ astrocytes after 3 hr of normoxia (CON) or OGD/REOX. In some OGD/REOX studies, cells were exposed to 5 μM bumetanide throughout the entire OGD/REOX and Ca^{2+} release experiment. Data points are the average of 20 cells from a representative experiment. Inset, Summary of peak thapsigargin-induced Ca^{2+} release data for 3 hr of normoxia (CON) or OGD/REOX with and without 5 μM bumetanide. Data are means ± SEM; $n = 4–6$; $^{*}p < 0.05$ versus CON; $^{\#}p < 0.05$ versus OGD/REOX. The arrow indicates the addition of thapsigargin. *C*, Cell mortality was assessed in NKCC1$^{+/+}$ astrocytes by PI and calcein AM staining after 2 hr of OGD, 2 hr of OGD plus 1 hr of REOX, 8 hr of OGD, or normoxic control conditions. Data are means ± SEM; $n = 2–6$. Inset, Intracellular ATP content was determined using a luminescence ATP detection assay after 2 hr of OGD and 1 hr of REOX, 8 hr of OGD, or normoxic control conditions. ATP content is expressed as nanomoles of ATP per milligram of protein. Data are means ± SEM; $n = 4–9$; $^{*}p < 0.05$ versus CON.

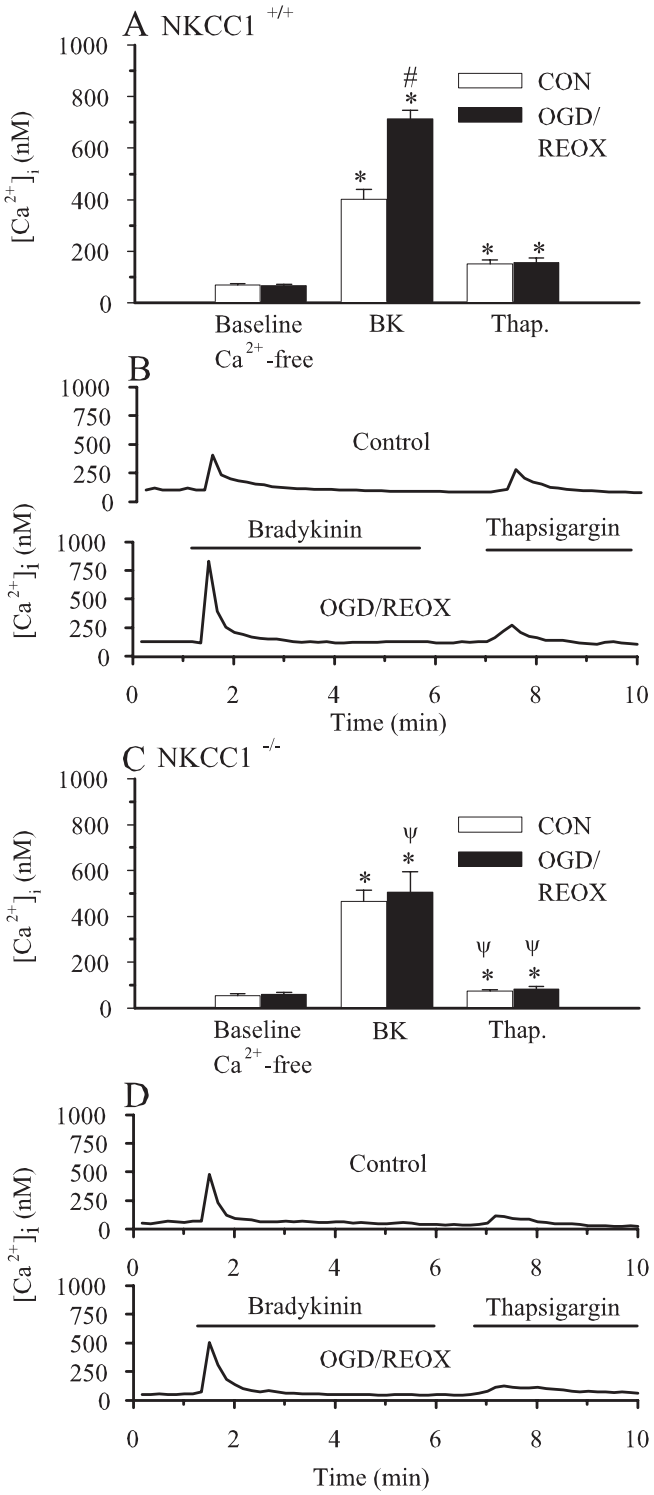

Figure 7. Increase in bradykinin-evoked Ca^{2+} release in NKCC1 $^{+/+}$ astrocytes but not in NKCC1 $^{-/-}$ astrocytes after OGD/REOX. Bradykinin-induced Ca^{2+} release was determined under Ca^{2+}-free conditions. NKCC1 $^{+/+}$ (*A*, *B*) and NKCC1 $^{-/-}$ (*C*, *D*) astrocytes were treated for either 3 hr of normoxia or OGD/REOX. Cells were exposed to $[Ca^{2+}]_o$-free buffer containing 1.0 μM bradykinin (BK) for 4.5 min, returned to $[Ca^{2+}]_o$-free buffer for 1 min, and then exposed to 1 μM thapsigargin (Thap) for 3 min. *A*, *C*, Summary of peak bradykinin and thapsigargin-induced Ca^{2+} release in NKCC1 $^{+/+}$ and NKCC1 $^{-/-}$ astrocytes, respectively. *B*, *D*, Representative single-cell Ca^{2+} responses in NKCC1 $^{+/+}$ (*B*) and NKCC1 $^{-/-}$ (*D*) astrocytes to bradykinin and thapsigargin. Data are means ± SEM; $n = 7$–12; $^{*}p < 0.05$ versus baseline control; $^{\#}p < 0.05$ versus normoxic control bradykinin; $^{\psi}p < 0.05$ versus NKCC1 $^{+/+}$.

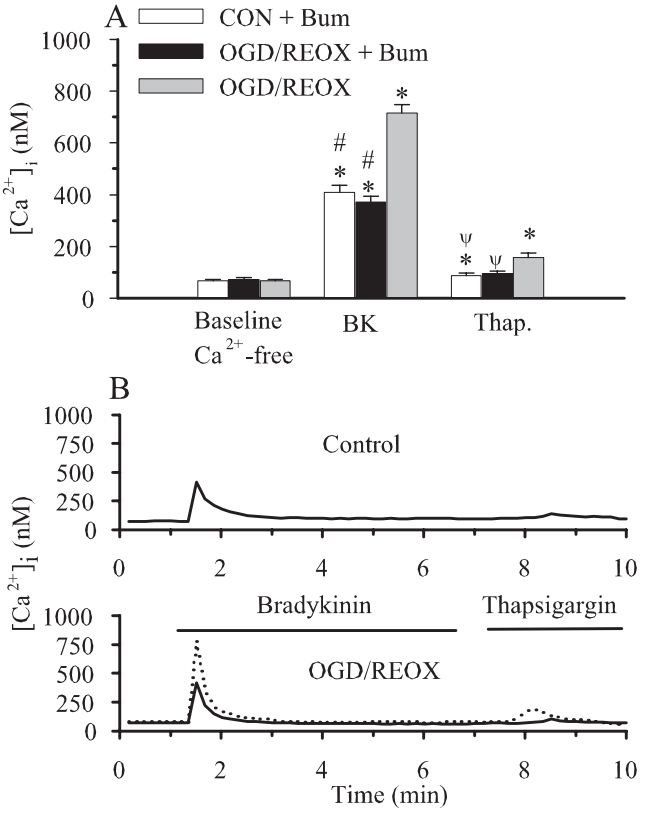

Figure 8. Bumetanide abolished an increase in Ca^{2+} transients in NKCC1 $^{+/+}$ astrocytes after OGD/REOX. Bradykinin-induced Ca^{2+} release was determined under Ca^{2+}-free conditions. NKCC1 $^{+/+}$ astrocytes were treated with 5 μM bumetanide (Bum) during either 3 hr of normoxic control (CON) or OGD/REOX. Bradykinin- or thapsigargin-evoked Ca^{2+} release was induced as described in Figure 7. *A*, Summary of peak bradykinin and thapsigargin (Thap.)-induced Ca^{2+} release in NKCC1 $^{+/+}$ astrocytes. Data from OGD/REOX-treated NKCC1 $^{+/+}$ astrocytes (Fig. 7*A*) are included to allow comparisons. *B*, Representative single-cell Ca^{2+} responses to bradykinin and thapsigargin. Dotted line, OGD/REOX-treated NKCC1 $^{+/+}$ astrocyte; solid line, bumetanide–OGD/REOX-treated NKCC1 $^{+/+}$ astrocyte. Data are means ± SEM; $n = 5$–12; $^{*}p < 0.05$ versus baseline control; $^{\#}p < 0.05$ versus OGD/REOX and bradykinin; $^{\psi}p < 0.05$ versus OGD/REOX and thapsigargin.

To confirm further that a lack of Ca^{2+} uptake by the intracellular Ca^{2+} stores in NKCC1 $^{-/-}$ astrocytes is indeed attributable to ablation of NKCC1 activity, we performed similar experiments with bumetanide. As shown in Figure 8*A*, 2 hr of OGD and 1 hr of REOX led to an enhanced filling of the intracellular bradykinin-sensitive Ca^{2+} stores in NKCC1 $^{+/+}$ astrocytes (714 ± 34 nM; $p < 0.05$). OGD/REOX treatment also resulted in a significant increase in the second Ca^{2+} release by thapsigargin (from 88 ± 9 to 156 ± 20 nM; $p < 0.05$) (Fig. 8*A*). In contrast, treatment of NKCC1 $^{+/+}$ astrocytes with bumetanide abolished the OGD-induced increase in Ca^{2+} transients mediated by either bradykinin or thapsigargin (Fig. 8*A*,*B*). This is consistent with the observations in NKCC1 $^{-/-}$ astrocytes.

Mitochondrial Ca^{2+} content in NKCC1 $^{+/+}$ astrocytes was moderately increased after OGD

Our data indicate that bradykinin-sensitive Ca^{2+} stores contain higher levels of Ca^{2+} after OGD. However, it is also possible that an increase in bradykinin-mediated Ca^{2+} release reflects a decrease in the efficiency of cytosolic Ca^{2+} clearance. Mitochondria are known to buffer increases in cytosolic Ca^{2+} after physiological and pathological stimuli. We therefore investigated whether Ca^{2+} loading in mitochondria of NKCC1 $^{+/+}$ astrocytes is af-

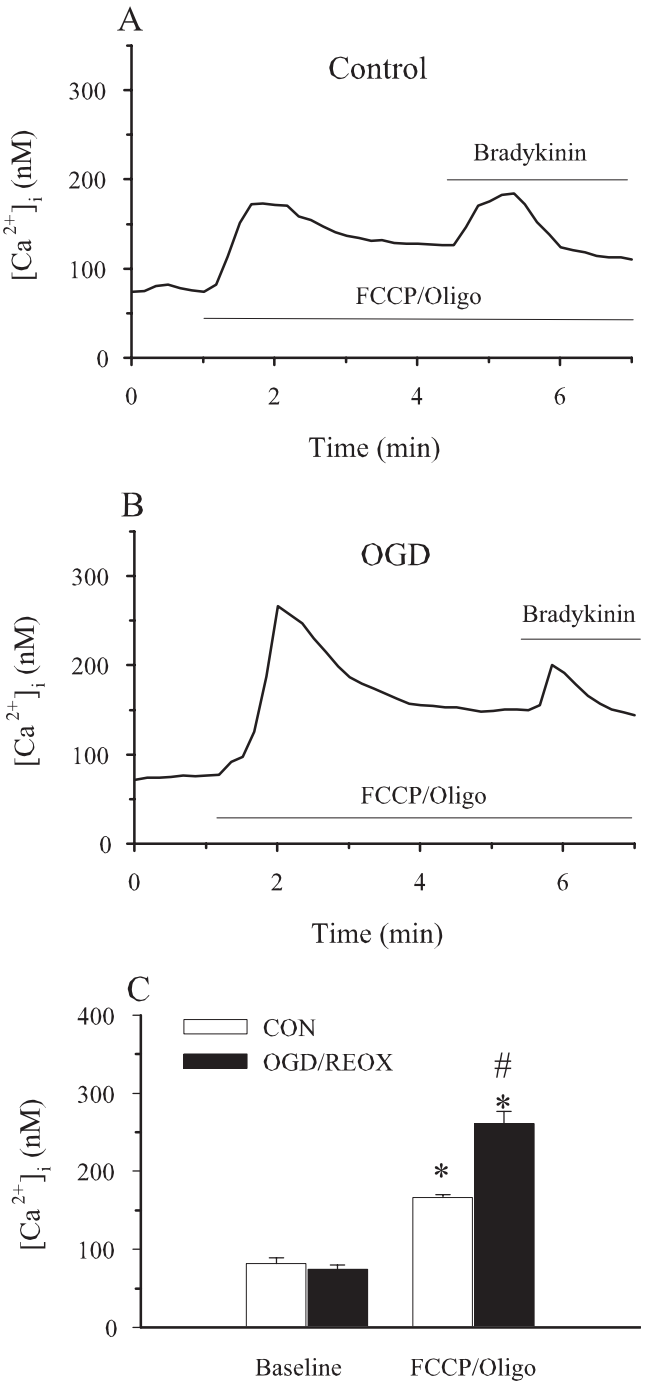

Figure 9. Moderate increase in mitochondrial Ca^{2+} content after OGD/REOX. FCCP/oligomycin (FCCP/Oligo)-induced Ca^{2+} release from mitochondria of NKCC1$^{+/+}$ astrocytes was determined under Ca^{2+}-free conditions. Astrocytes were exposed to 10 μM FCCP and 2.5 μg/ml oligomycin after either 3 hr of normoxia (CON) (*A*) or OGD/REOX (*B*). Cells were subsequently exposed to1 μM bradykinin. *A*, *B*, Representative Ca^{2+} responses in a single cell to FCCP/oligomycin followed by bradykinin under Ca^{2+}-free conditions. *C*, Summary of the peak $[Ca^{2+}]_i$ level induced by FCCP/oligomycin. Data are means ± SEM; $n = 4$; $^*p < 0.01$ versus baseline; $^{\#}p < 0.01$ versus control.

fected during OGD. NKCC1$^{+/+}$ astrocytes were exposed to 10 μM FCCP and 2.5 μg/ml oligomycin under Ca^{2+}-free conditions, after either 3 hr of normoxia (Fig. 9*A*) or 2 hr of OGD and 1 hr of REOX (Fig. 9*B*). After a 10–20 sec delay, $[Ca^{2+}]_i$ increased in response to FCCP/oligomycin in both normoxic and OGD/REOX-treated astrocytes (Fig. 9*A*,*B*), with a peak increase in $[Ca^{2+}]_i$ of 166 ± 4 nM under normoxic conditions and 261 ± 15 nM under OGD/REOX ($p < 0.05$) (Fig. 9*C*). The area under the Ca^{2+} transient was also determined in terms of arbitrary units (AU; Ca^{2+} concentration × minutes) and significantly greater in OGD/REOX-treated astrocytes (177 ± 15 AU) than in normoxic controls (84 ± 13 AU; $n = 4$; $p < 0.01$). This suggests that mitochondrial buffering of Ca^{2+} is only moderately increased after OGD/REOX and has not yet reached its capacity (250–1000 nM) (Babcock et al., 1997). On the other hand, the increases in Ca^{2+} release induced by OGD/REOX were three times greater from bradykinin-sensitive stores than from mitochondria (Figs. 8*A*, 9*C*). This implies that the intracellular stores are more active in buffering Ca^{2+} overload after OGD/REOX than mitochondria in the current study.

We examined further bradykinin-induced Ca^{2+} release from intracellular stores when mitochondrial Ca^{2+} buffering ability is blocked by FCCP–oligomycin. However, as shown in Figure 9, *A* and *B*, bradykinin-mediated Ca^{2+} release was significantly reduced in the presence of FCCP–oligomycin in both normoxia- and OGD/REOX-treated NKCC1$^{+/+}$ astrocytes. This is consistent with a report that inhibition of mitochondrial ATP production affects Ca^{2+} loading in astrocyte Ca^{2+} stores (Kahlert and Reiser, 2000). Thus, we were unable to characterize bradykinin-induced Ca^{2+} release in the absence of mitochondrial Ca^{2+} buffering function.

Inhibition of the reverse-mode operation of NCX abolished OGD-induced increase in Ca^{2+} transients

An increase in bradykinin-evoked Ca^{2+} release after OGD/REOX may reflect a stimulation of Ca^{2+} entry via the reverse-mode activity of NCX as a result of accumulation of intracellular Na^+. To investigate further the role of NCX in the OGD/REOX-induced increase in Ca^{2+} store filling, we used KB-R7943, an inhibitor of the reverse-mode operation of NCX activity. First, we established that KB-R7943 blocked the reverse-mode operation of NCX in a dose-dependent manner (Fig. 10*A–C*). The reverse-mode operation of NCX was induced by exposing cells to a Na^+- and Ca^{2+}-free buffer to reduce $[Na^+]_i$ and subsequently to an Na^+-free buffer containing Ca^{2+} (Fig. 10*A*, a,b). The reverse-mode operation of NCX triggered an abrupt increase in $[Ca^{2+}]_i$. After returning to HEPES–MEM, $[Ca^{2+}]_i$ quickly recovered to baseline values. The reverse-mode operation of NCX can be stimulated repeatedly (Fig. 10*A*). However, when the cell was exposed to 10 μM KB-R7943, the reverse-mode operation of NCX was inhibited (Fig. 10*A*).

The dose-dependent effect of KB-R7943 on the reverse-mode operation of NCX was determined (Fig. 10*B*). A plot of percentage of inhibition versus KB-R7943 concentration was fit with a hyperbolic equation that yielded an IC_{50} value of 0.88 μM (Fig. 10*C*). This is similar to the IC_{50} values reported previously for Na^+-dependent Ca^{2+} influx inhibition by KB-R7943: 0.32 μM in guinea pig cardiac ventricular cells (Watano et al., 1996), 1.6 μM for cardiac NCX1-transfected CCL39 cells (Iwamoto et al., 1996), and 2.4 μM for rat cardiomyocytes (Iwamoto et al., 1996).

Subsequently, we investigated whether inhibition of NCX with KB-R7943 would reduce Ca^{2+} entry and subsequently Ca^{2+} uptake via Ca^{2+} stores. Three micromolar KB-R7943 (86% inhibition of NCX) (Fig. 10*C*) was used in these studies because cell damage occurred with prolonged incubation with 10 μM KB-R7943 in our pilot study (data not shown). Bradykinin triggered a peak release of Ca^{2+} in normoxic control cells (407 ± 48 nM $[Ca^{2+}]_i$) (Fig. 10*D*). Similar to data in Figure 7, after 2 hr of OGD and 1 hr of REOX, bradykinin-evoked Ca^{2+} release reached 750 ± 35 nM in NKCC1$^{+/+}$ astrocytes (Fig. 10*D*). In contrast, in

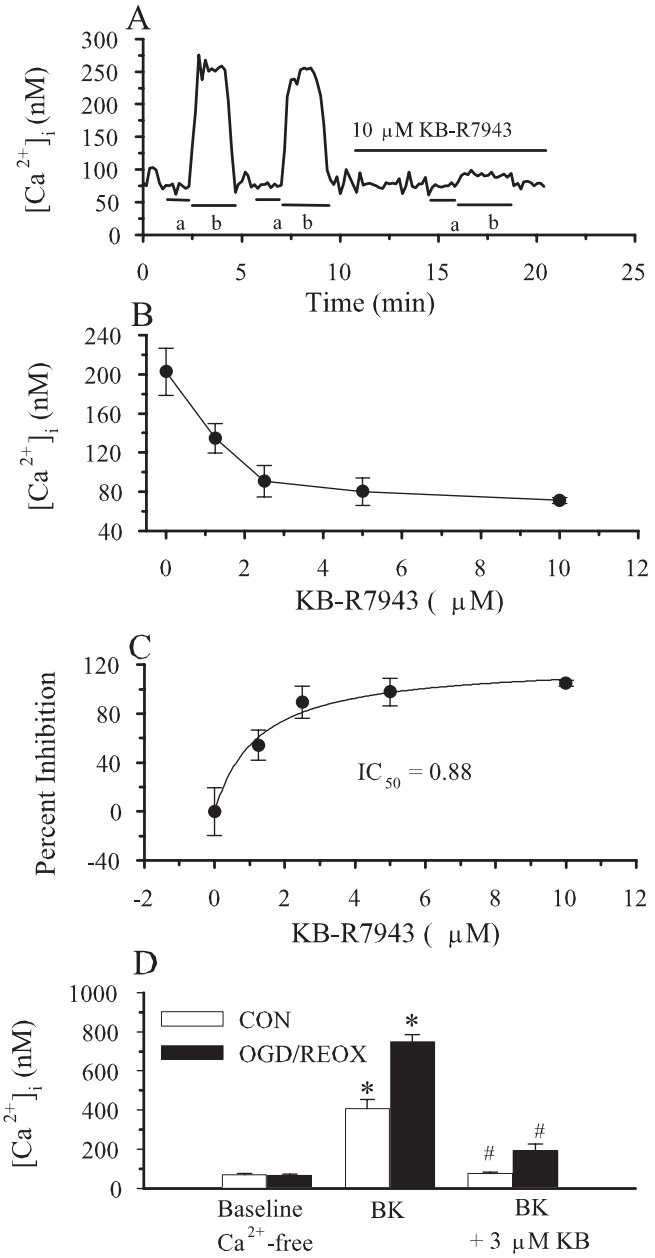

Figure 10. Inhibition of the Na^+/Ca^{2+} exchanger abolished OGD-induced increase in Ca^{2+} release. The effect of KB-R7943 on reverse-mode activity of NCX was investigated in NKCC1 $^{+/+}$ astrocytes. *A*, The reverse-mode operation of NCX was induced by exposing cells to an Na^+- and Ca^{2+}-free buffer (a, 1 min) followed by Na^+-free buffer that contained Ca^{2+} (b, 2 min). After a brief (1 min) return to normal HEPES–MEM, cells were treated repeatedly with the same protocol, which resulted in similar levels of Ca^{2+} rise. However, in the presence of 10 μM KB-R7943, the reverse-mode operation of NCX failed to increase $[Ca^{2+}]_i$. *B*, *C*, Similar experiments were performed in the presence of varying concentrations of KB-R7943 (0–10 μM). Data are means ± SEM of 20 cells from a single coverslip for each level of KB-R7943; $n = 2$. Filled circles indicate control conditions. *D*, Effect of 3 μM KB-R7943 on bradykinin-induced Ca^{2+} release in NKCC1 $^{+/+}$ astrocytes during OGD/REOX or 3 hr of normoxic control (CON). For KB-R7943 treatment, 3 μM KB-R7943 was present during normoxia or OGD/REOX. Baseline measurements were performed in a Ca^{2+}-free buffer. Data are means ± SEM; $n = 5$; $^*p <$ 0.05 versus baseline control; $^\#p < 0.05$ versus bradykinin treatment.

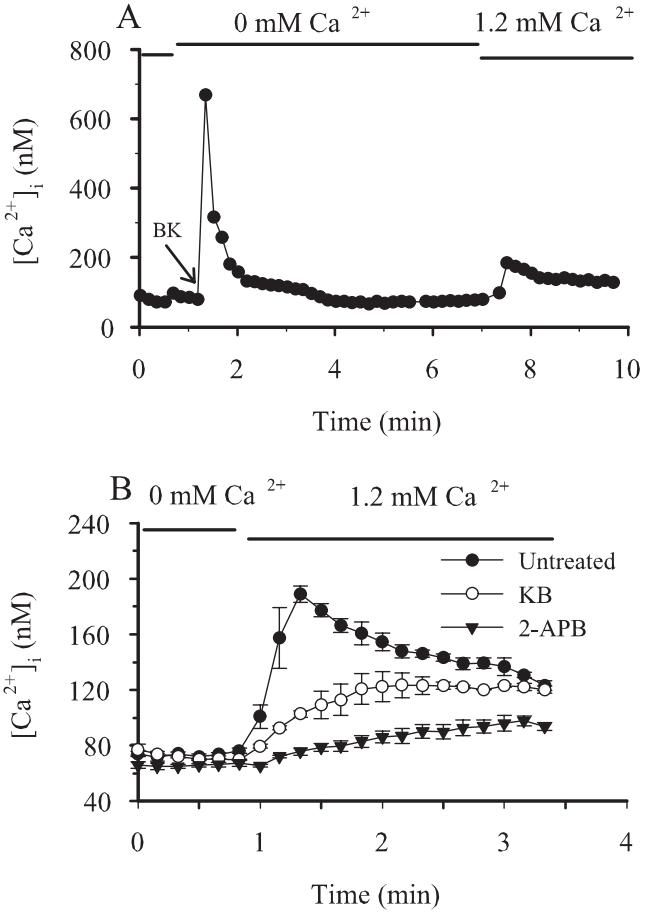

Figure 11. Differential effect of the Na^+/Ca^{2+} exchanger inhibition on store-operated calcium entry after OGD/REOX. The activity of SOCE after depletion of intracellular Ca^{2+} stores was investigated. *A*, After 2 hr of OGD and 1 hr of REOX (filled circles), NKCC1 $^{+/+}$ astrocytes were exposed to 1 μM bradykinin (arrow) under $[Ca^{2+}]_o$-free conditions to empty intracellular Ca^{2+} stores. Cells were subsequently exposed to a buffer containing 1.2 mM $[Ca^{2+}]_o$, which initiated Ca^{2+} entry. Data are the mean of 20 cells from one experiment. *B*, Effects of KB R7943 or SOCE channel blocker 2-APB on SOCE. After bradykinin exposure (as in *A*), cells were exposed to Ca^{2+}-free buffer (untreated) or Ca^{2+}-free buffer containing either 3 μM KB-R7943 or 50 μM 2-APB for 1–2 min. Cells were then exposed to HEPES–MEM (1.2 mM $[Ca^{2+}]_o$) or the same buffer containing either 3 μM KB-R7943 (KB) or 50 μM 2-APB. Data are means ± SEM; $n = 4$.

the presence of 3 μM KB-R7943, bradykinin-evoked Ca^{2+} release was reduced by 82% during 2 hr of OGD and 1 hr of REOX and by 98% in normoxic cells, in which $[Ca^{2+}]_i$ levels were essentially the same under baseline conditions or after treatment with bradykinin. These findings suggest that the reverse-mode operation of NCX contributes to the loading of bradykinin-sensitive Ca^{2+} stores in astrocytes during OGD and REOX.

Differential effects of KB-R7943 and store-operated Ca^{2+} entry channel inhibitor 2-APB on $[Ca^{2+}]_i$ after OGD/REOX

In our present study, we believe that the primary mechanism underlying KB-R7943-mediated reduction of Ca^{2+} uptake in ER (shown above) is through inhibition of NCX. This is because these experiments were performed in the absence of extracellular Ca^{2+}; thus, other channels such as store-operated Ca^{2+} entry (SOCE) were inactive.

However, it was reported that 5 μM KB-R7943 reduced SOCE by ~30% in astrocytes (Arakawa et al., 2000). To investigate further whether 3 μM KB-R7943 would cause effects on SOCE, we compared the effects of KB-R7943 and SOCE channel inhibitor 2-APB on $[Ca^{2+}]_i$ after 2 hr of OGD and 1 hr of REOX. When NKCC1 $^{+/+}$ cells were exposed to 1 μM bradykinin in a Ca^{2+}-free buffer, there was a large transient increase in $[Ca^{2+}]_i$ (Fig. 11*A*). Within 2–3 min, the increase in intracellular Ca^{2+} was cleared from the cell. As the cells were exposed to a 1.2 mM Ca^{2+} buffer,

store-operated Ca^{2+} influx was initiated, and $[Ca^{2+}]_i$ increased by ~2.5-fold (<40 sec), which gradually declined over the next 2 min (Fig. 11*B*). In the presence of 2-APB, cells showed no significant increase in $[Ca^{2+}]_i$ at <40 sec (Fig. 11*B*). The $[Ca^{2+}]_i$ remained within normal values for baseline $[Ca^{2+}]_i$, although it tended to slowly increase over the next 2 min. This suggests that 2-APB abolished store-operated Ca^{2+} influx in astrocytes. In contrast, KB-R7943 treatment resulted in a sharp reduction in the initial rise of store-operated Ca^{2+} influx. However, over the next 2 min, $[Ca^{2+}]_i$ continued to increase in the KB-R7943-treated cells and eventually reached levels similar to those in untreated cells. Thus, KB-R7943-mediated effects can be differentiated from those of 2-APB, implying that 3 μM KB-R7943 does not effectively inhibit SOCE.

Discussion

Stimulation of NKCC1 activity after OGD

In the current study, we found that NKCC1-mediated ^{86}Rb influx was significantly increased in both $NKCC1^{+/+}$ and $NKCC1^{+/-}$ astrocytes after OGD. In addition, OGD also caused increased levels of phosphorylated NKCC1 protein in $NKCC1^{+/+}$ astrocytes, recognized by the phosphospecific Thr^{184}/Thr^{189} NKCC antibody. No changes in total NKCC1 protein expression were detected in $NKCC1^{+/+}$ astrocytes after OGD. Phosphorylation-dependent stimulation of NKCC1 activity has been shown in numerous experimental systems using various stimuli (Lytle and Forbush, 1992; Russell, 2000). The three threonines (Thr^{184}, Thr^{189}, and Thr^{202}) on the N-terminal regulatory domain of NKCC1 modulate NKCC1 activity in species ranging from shark to human (Flemmer et al., 2002). Phosphorylation of Thr^{184}/Thr^{189} correlates with NKCC1 activation in epithelial cells (Darman and Forbush, 2002). Such a correlation has also been found in cultured cortical neurons when intracellular Cl^- is reduced (Schomberg et al., 2003). Together, our study demonstrates that OGD induces phosphorylation of NKCC1 and stimulation of NKCC1 activity in cortical astrocytes.

The identity of the kinases responsible for the phosphorylation of NKCC1 in astrocytes after OGD is unknown. Recently, OSR1 (oxidative stress response kinase) and SPAK (STE20/SPS-1-related, proline–alanine-rich kinase), along with its rat homolog PASK (proline-alanine-rich STE20-related kinase), were found to bind to the third conserved domain in the NKCC1 N terminus and coimmunoprecipitated with NKCC1 protein (Piechotta et al., 2002; Dowd and Forbush, 2003). Overexpression of PASK in human embryonic kidney cells causes a small but significant increase in NKCC1 activity, and the phosphorylation of PASK coincides with that of NKCC1 (Dowd and Forbush, 2003).

PASK and SPAK are preferentially expressed in the brain and in cells that are active in ion transport and rich in Na^+/K^+–ATPase (Ushiro et al., 1998; Johnston et al., 2000; Piechotta et al., 2002). SPAK activates the p38 MAP kinase pathway and has been suggested to play a role in initiation of the cellular stress responses (Johnston et al., 2000). Although PASK and SPAK have been found in neurons, their location in astrocytes has not been reported. However, Fray, a *Drosophila* serine–threonine kinase that is homologous to mammalian PASK, is expressed in peripheral glia, and its function is required for normal axonal ensheathment (Leiserson et al., 2000). Additional studies will be required to determine whether the proline–alanine-rich STE20-related kinase mediates the observed phosphorylation and stimulation of NKCC1 in astrocytes after OGD.

NKCC1-mediated Na^+ entry and an effect on Ca^{2+} homeostasis

Pathological insults such as anoxia and ischemia are characterized by changes in ion homeostasis, including intracellular Na^+ accumulation. In the current study, we found that OGD led to an ~3.6-fold increase in $[Na^+]_i$. This finding is consistent with a report on $[Na^+]_i$ accumulation in spinal cord astrocytes induced by glucose deprivation, chemical hypoxia, and simulated ischemia (Rose et al., 1998). Ischemia-mediated Na^+ accumulation in astrocytes has been attributed to a reduction in Na^+/K^+–ATPase activity and activation of Na^+ channels (Rose et al., 1998; Stys, 1998). Our data show that inhibition of NKCC1 blocked ~80% of the Na^+ loading. The remaining Na^+ accumulation could be the result of a decrease in Na^+/K^+–ATPase activity because its activity was reduced by ~30% in astrocytes after OGD (Fig. 2). In addition, either genetic ablation or pharmacological inhibition of NKCC1 abolished OGD-mediated Cl^- influx and swelling. Thus, these data provide the first line of evidence that NKCC1 plays a pivotal role in Na^+ homeostasis in cortical astrocytes after OGD.

The mechanisms of glial ischemic injury include Ca^{2+} entry and Ca^{2+}-mediated cell death. The Ca^{2+} entry pathways involve L-type voltage-gated Ca^{2+} channels, AMPA and metabotropic glutamate receptors, and reverse operation of the NCX (Stys, 1998). In the current study, we detected an increase in bulk cytosolic $[Ca^{2+}]$ in astrocytes after OGD in the presence of thapsigargin. Moreover, Ca^{2+} release from bradykinin-sensitive Ca^{2+} stores was increased by ~78% in $NKCC1^{+/+}$ astrocytes after OGD. This implies that Ca^{2+} entry was elevated after OGD and Ca^{2+} stores subsequently buffered $[Ca^{2+}]_i$. Inhibition of reverse operation of NCX with 3 μM KB-R7943 abolished the OGD-mediated increase in releasable Ca^{2+} in bradykinin-sensitive Ca^{2+} stores. These findings suggest that reverse operation of NCX plays a role in Ca^{2+} entry and Ca^{2+} signaling in cortical astrocytes after OGD.

It is generally accepted that inhibition of the Na^+/K^+–ATPase and reduction of the $[Na^+]$ gradient across the plasma membrane promote Ca^{2+} entry via NCX in most types of cells (Blaustein and Lederer, 1999). Recently, it has been suggested that NCX and the Na^+/K^+–ATPase ($\alpha 2$ or $\alpha 3$ subunits) are confined to the same plasma membrane microdomains. Thus, NCX may be regulated by Na^+/K^+–ATPase activity via its influence on the Na^+ electrochemical gradient across the plasma membrane (Golovina et al., 2003). Reduction in Na^+/K^+–ATPase activity elevates local $[Na^+]_i$, which in turn activates the Ca^{2+} entry via NCX and enhances filling of the ER Ca^{2+} stores (Golovina et al., 2003). In the current study, we observed for the first time that prevention of NKCC1-mediated Na^+ accumulation in astrocytes can also inhibit Ca^{2+} entry via NCX and subsequently decreases loading of intracellular Ca^{2+} stores. This suggests that the functions of NKCC1 and NCX may be closely associated, as has been proposed for NCX and the Na^+/K^+–ATPase. Thus, both the $Na+/K^+$–ATPase and NKCC1 may be involved in regulating intracellular Na^+ homeostasis, which in turn affects NCX activity and Ca^{2+} signaling in astrocytes. In addition, in a recent report (Rosker et al., 2004), activation of the TRPC3 (transient receptor potential subfamily) cation channel causes Na^+ loading. The Na^+ entry and membrane depolarization subsequently lead to a rise in $[Ca^{2+}]_i$ via shifting NCX to the reverse mode. This is similar to our proposed scenario that NKCC1 mediates Na^+ accumulation during OGD/REOX, which triggers reverse operation of NCX. Moreover, 5 μM KB-R7943

had no effects on the typical TRPC3-mediated inward Na^+ currents (Rosker et al., 2004).

Two classes of spatially resolved ER Ca^{2+} stores, cyclopiazonic acid (CPA)-sensitive and caffeine–ryanodine-sensitive, have been found in rat cortical astrocytes (Golovina and Blaustein, 2000). The CPA-sensitive Ca^{2+} stores release Ca^{2+} in response to an agonist and IP_3-mediated Ca^{2+} signaling cascade, whereas caffeine–ryanodine trigger Ca^{2+}-induced Ca^{2+} entry. In the current study, we observed both bradykinin-sensitive and -insensitive Ca^{2+} release in mouse cortical astrocytes. This may reflect the CPA- and caffeine–ryanodine-sensitive Ca^{2+} stores, respectively. Interestingly, OGD/REOX treatment of NKCC1$^{+/+}$ astrocytes led to an increase in Ca^{2+} sequestration in both Ca^{2+} stores. Either pharmacological inhibition or genetic ablation of NKCC1 abolished the OGD/REOX-induced increase in the Ca^{2+} sequestration. Thus, it is possible that NKCC1-mediated Na^+ accumulation during OGD indirectly affects both Ca^{2+} stores.

Table 2. Thermodynamic analysis of NKCC1 during OGD/REOX, HAIR, and HAIR/REOX

	Ionic concentrations (mM)						
	$[Na^+]_i$	$[Na^+]_o$	$[K^+]_i$	$[K^+]_o$	$[Cl^-]_i$	$[Cl^-]_o$	ΔG
Control	12.7	137	112	5.4	36	144	−12.3
OGD/REOX	46	135	112	5.6	36	135	−8.9
OGD/REOX[a]	46	135	56	5.6	72	135	−8.9
HAIR	8	50	112	62	36	57	−12.5
HAIR/REOX[a]	52	137	56	5.4	72	144	−8.9

[a] $[Cl^-]_i$ is assumed to increase by 2×, $[K^+]_i$ is assumed to decrease by 2×.

ΔG of NKCC1 under various ionic conditions was calculated using the following equation:

$$\Delta G = RT\,1n\frac{[Na^+]_i \times [K^+]_i \times [Cl^-]_i^2}{[Na^+]_o \times [K^+]_o \times [Cl^-]_o^2}.$$

RT at 22°C is 2.45 kJ/mmol.

Thermodynamic analysis of NKCC1 and NCX under ischemic conditions

We calculated the net free energy (ΔG) for NKCC1 activity, as determined by the concentration gradients of the three ions (Russell, 2000), and investigated whether changes in ΔG during OGD/REOX would allow for NKCC1 to mediate Na^+ accumulation. As shown in Table 2, we calculated the ΔG for NKCC1 using the known concentrations of $[Na^+]_o$, $[Na^+]_i$, $[K^+]_o$, and $[Cl^-]_o$ and assumed concentrations for $[K^+]_i$ and $[Cl^-]_i$ of 111 and 36 mM, respectively. Under control conditions, ΔG was quite negative, indicating that net uptake of Na^+ was strongly favored (Table 2). During OGD/REOX, ΔG decreased by 28% (assuming no changes in $[K^+]_i$ and $[Cl^-]_i$), and the net direction of Na^+ remained strongly inward (Table 2). Furthermore, if it is assumed that during OGD/REOX, $[K^+]_i$ decreased by one-half and $[Cl^-]_i$ doubled, there is no effect on the calculated ΔG (Table 2). Similar results were also obtained under conditions of HAIR and HAIR/REOX, in which the known concentrations of $[Na^+]_o$, $[Na^+]_i$, $[K^+]_o$, and $[Cl^-]_o$ were substituted in the calculations (Table 2).

An additional important question to consider is whether the thermodynamics of NCX during OGD/REOX would make accumulation of Ca^{2+} possible. Ca^{2+} can be transported via NCX either into or out of the cell, depending on the difference between the membrane potential and the reversal potential ($E_{Na/Ca}$) of NCX (Blaustein and Lederer, 1999). $E_{Na/Ca}$ is defined as $E_{Na/Ca} = 3 \times E_{Na} - 2 \times E_{Ca}$, where $E_{Na} = (RT/F) \times \ln([Na^+]_o/[Na^+]_i)$, and $E_{Ca} = (RT/2F) \times \ln([Ca^{2+}]_o/[Ca^{2+}]_i)$ (Blaustein and Lederer, 1999). If RT/F is considered to be 57 at 22°C, then $E_{Na/Ca}$ can be calculated as approximately −65 mV using the concentrations for $[Na^+]_o$, $[Na^+]_i$, $[Ca^{2+}]_o$, and $[Ca^{2+}]_i$ in NKCC1$^{+/+}$ astrocytes. Under control conditions in which the plasma membrane potential (V_m) averages about −60 mV (McKhann et al., 1997), the difference between V_m and $E_{Na/Ca}$ is small and there is little flux through NCX. However, V_m of cultured cortical astrocytes is highly heterogeneous (−22 to −82 mV) (McKhann et al., 1997). It can be expected that when V_m is more negative in respect to $E_{Na/Ca}$, Ca^{2+} ions would be driven out of cells.

In the presence of the ionic concentrations under OGD/REOX conditions, $E_{Na/Ca}$ would become more negative (approximately −160 mV), which favors the net influx of Ca^{2+} at constant V_m. Although we did not measure V_m under OGD/REOX conditions, we speculate that the average V_m is likely to be depolarized (Duffy and MacVicar, 1994). The estimated influx of Ca^{2+} via the reversal of NCX, at depolarized V_m (−20 mV) and increased $[Na^+]i$ (~40 mM), could be ~1000 nM. This is similar to our measured $[Ca^{2+}]_i$ values under OGD/REOX conditions. Together, from a thermodynamic point of view, there is no reason to a priori rule out reversal of NCX during OGD/REOX.

References

Alvarez-Leefmans FJ (2001) Intracellular chloride regulation. In: Cell physiology sourcebook: a molecular approach (Sperelakis N, ed), pp 301–318. San Diego: Academic.

Arakawa N, Sakaue M, Yokoyama I, Hashimoto H, Koyama Y, Baba A, Matsuda T (2000) KB-R7943 inhibits store-operated Ca^{2+} entry in cultured neurons and astrocytes. Biochem Biophys Res Commun 279:354–357.

Babcock DF, Herrington J, Goodwin PC, Park YB, Hille B (1997) Mitochondrial participation in the intracellular Ca^{2+} network. J Cell Biol 136:833–844.

Blaustein MP, Lederer WJ (1999) Sodium/calcium exchange: its physiological implications. Physiol Rev 79:763–854.

Bondarenko A, Chesler M (2001) Rapid astrocyte death induced by transient hypoxia, acidosis, and extracellular ion shifts. Glia 34:134–142.

Darman RB, Forbush B (2002) A regulatory locus of phosphorylation in the N terminus of the Na-K-Cl cotransporter, NKCC1. J Biol Chem 277:37542–37550.

Dowd BF, Forbush B (2003) PASK (proline-alanine-rich STE20-related kinase), a regulatory kinase of the Na-K-Cl cotransporter (NKCC1). J Biol Chem 278:27347–27353.

Duffy S, MacVicar BA (1994) Potassium-dependent calcium influx in acutely isolated hippocampal astrocytes. Neuroscience 61:51–61.

Flagella M, Clarke LL, Miller ML, Erway LC, Giannella RA, Andringa A, Gawenis LR, Kramer J, Duffy JJ, Doetschman T, Lorenz JN, Yamoah EN, Cardell EL, Shull GE (1999) Mice lacking the basolateral Na-K-2Cl cotransporter have impaired epithelial chloride secretion and are profoundly deaf. J Biol Chem 274:26946–26955.

Flemmer AW, Gimenez I, Dowd BF, Darman RB, Forbush B (2002) Activation of the Na-K-Cl cotransporter NKCC1 detected with a phospho-specific antibody. J Biol Chem 277:37551–37558.

Goldman WF, Yarowsky PJ, Juhaszova M, Krueger BK, Blaustein MP (1994) Sodium/calcium exchange in rat cortical astrocytes. J Neurosci 14:5834–5843.

Golovina VA, Blaustein MP (2000) Unloading and refilling of two classes of spatially resolved endoplasmic reticulum Ca^{2+} stores in astrocytes. Glia 31:15–28.

Golovina VA, Song H, James PF, Lingrel JB, Blaustein MP (2003) Na^+ pump alpha 2-subunit expression modulates Ca^{2+} signaling. Am J Physiol 284:C475–C486.

Grynkiewicz G, Poenie M, Tsien RY (1985) A new generation of Ca^{2+} indicators with greatly improved fluorescence properties. J Biol Chem 260:3440–3450.

Hamann S, Kiilgaard JF, Litman T, Alvarez-Leefmans FJ, Winther BR, Zeuthen T (2002) Measurement of cell volume changes by fluorescence self-quenching. J Fluor 12:139–145.

Haworth RA, Redon D (1998) Calibration of intracellular Ca transients of isolated adult heart cells labelled with fura-2 by acetoxymethyl ester loading. Cell Calcium 24:263–273.

Hoppe D, Kettenmann H (1989) GABA triggers a Cl^- efflux from cultured mouse oligodendrocytes. Neurosci Lett 97:334–339.

Iwamoto T, Watano T, Shigekawa M (1996) A novel isothiourea derivative selectively inhibits the reverse mode of Na^+/Ca^{2+} exchange in cells expressing NCX1. J Biol Chem 271:22391–22397.

Johnston AM, Naselli G, Gonez LJ, Martin RM, Harrison LC, DeAizpurua HJ (2000) SPAK, a STE20/SPS1-related kinase that activates the p38 pathway. Oncogene 19:4290–4297.

Kahlert S, Reiser G (2000) Requirement of glycolytic and mitochondrial energy supply for loading of Ca^{2+} stores and $InsP_3$-mediated Ca^{2+} signaling in rat hippocampus astrocytes. J Neurosci Res 61:409–420.

Laemmli UK (1970) Cleavage of structural proteins during the assembly of the head of bacteriophage T4. Nature 227:680–685.

Leiserson WM, Harkins EW, Keshishian H (2000) Fray, a *Drosophila* serine/threonine kinase homologous to mammalian PASK, is required for axonal ensheathment. Neuron 28:793–806.

Li S, Jiang Q, Stys PK (2000) Important role of reverse Na^+-Ca^{2+} exchange in spinal cord white matter injury at physiological temperature. J Neurophysiol 84:1116–1119.

Longuemare MC, Rose CR, Farrell K, Ransom BR, Waxman SG, Swanson RA (1999) K^+-induced reversal of astrocyte glutamate uptake is limited by compensatory changes in intracellular Na^+. Neuroscience 93:285–292.

Lytle C, Forbush B (1992) The Na-K-Cl cotransport protein of shark rectal gland. II. Regulation by direct phosphorylation. J Biol Chem 267:25438–25443.

Lytle C, Xu JC, Biemesderfer D, Forbush III B (1995) Distribution and diversity of Na-K-Cl cotransport proteins: a study with monoclonal antibodies. Am J Physiol 269:C1496–C1505.

McKhann GM, D'Ambrosio R, Janigro D (1997) Heterogeneity of astrocyte resting membrane potentials and intercellular coupling revealed by whole-cell and gramicidin-perforated patch recordings from cultured neocortical and hippocampal slice astrocytes. J Neurosci 17:6850–6863.

Petr MJ, Wurster RD (1997) Determination of *in situ* dissociation constant for Fura-2 and quantitation of background fluorescence in astrocyte cell line U373-MG. Cell Calcium 21:233–240.

Piechotta K, Lu J, Delpire E (2002) Cation chloride cotransporters interact with the stress-related kinases Ste20-related proline-alanine-rich kinase (SPAK) and oxidative stress response 1 (OSR1). J Biol Chem 277:50812–50819.

Rose CR, Waxman SG, Ransom BR (1998) Effects of glucose deprivation, chemical hypoxia, and simulated ischemia on Na^+ homeostasis in rat spinal cord astrocytes. J Neurosci 18:3554–3562.

Rosker C, Graziani A, Lukas M, Eder P, Zhu MX, Romanin C, Groschner K (2004) Ca^{2+} signaling by TRPC3 involves Na^+ entry and local coupling to the Na^+/Ca^{2+} exchanger. J Biol Chem 279:13696–13704.

Russell JM (2000) Sodium-potassium-chloride cotransport. Physiol Rev 80:211–276.

Schomberg SL, Su G, Haworth RA, Sun D (2001) Stimulation of Na-K-2Cl cotransporter in neurons by activation of non-NMDA ionotropic receptor and group-I mGluRs. J Neurophysiol 85:2563–2575.

Schomberg SL, Bauer J, Kintner DB, Su G, Flemmer A, Forbush B, Sun D (2003) Cross talk between the $GABA_A$ receptor and the Na-K-Cl cotransporter is mediated by intracellular Cl^-. J Neurophysiol 89:159–167.

Siesjö BK (1992) Pathophysiology and treatment of focal cerebral ischemia. Part I: pathophysiology. J Neurosurg 77:169–184.

Silver IA, Deas J, Erecinska M (1997) Ion homeostasis in brain cells: differences in intracellular ion responses to energy limitation between cultured neurons and glial cells. Neuroscience 78:589–601.

Smith IF, Boyle JP, Plant LD, Pearson HA, Peers C (2003) Hypoxic remodeling of Ca^{2+} stores in type I cortical astrocytes. J Biol Chem 278:4875–4881.

Smith JP, Cunningham LA, Partridge LD (2000) Coupling of AMPA receptors with the Na^+/Ca^{2+} exchanger in cultured rat astrocytes. Brain Res 887:98–109.

Stys PK (1998) Anoxic and ischemic injury of myelinated axons in CNS white matter: from mechanistic concepts to therapeutics. J Cereb Blood Flow Metab 18:2–25.

Su G, Haworth RA, Dempsey RJ, Sun D (2000) Regulation of Na^+-K^+-Cl^- cotransporter in primary astrocytes by dibutyryl cAMP and high $[K^+]_o$. Am J Physiol 279:C1710–C1721.

Su G, Kintner DB, Sun D (2002a) Contribution of $Na^+K^+Cl^-$ cotransporter to high $[K^+]_o$-induced swelling and EAA release in astrocytes. Am J Physiol 282:C1136–C1146.

Su G, Kintner DB, Flagella M, Shull GE, Sun D (2002b) Astrocytes from Na^+-K^+-Cl^- cotransporter-null mice exhibit absence of swelling and decrease in EAA release. Am J Physiol 282:C1147–C1160.

Sun D, Murali SG (1999) Na^+-K^+-$2Cl^-$ cotransporter in immature cortical neurons: a role in intracellular Cl^- regulation. J Neurophysiol 81:1939–1948.

Swanson RA, Liu J, Miller JW, Rothstein JD, Farrell K, Stein BA, Longuemare MC (1997) Neuronal regulation of glutamate transporter subtype expression in astrocytes. J Neurosci 17:932–940.

Ushiro H, Tsutsumi T, Suzuki K, Kayahara T, Nakano K (1998) Molecular cloning and characterization of a novel Ste20-related protein kinase enriched in neurons and transporting epithelia. Arch Biochem Biophys 355:233–240.

Walz W (1989) Role of glial cells in the regulation of the brain ion microenvironment. Prog Neurobiol 33:309–333.

Wang H, Yan Y, Kintner DB, Lytle C, Sun D (2003) GABA-mediated trophic effect on oligodendrocytes requires Na-K-2Cl cotransport activity. J Neurophysiol 90:1257–1265.

Watano T, Kimura J, Morita T, Nakanishi H (1996) A novel antagonist, No. 7943, of the Na^+/Ca^{2+} exchange current in guinea-pig cardiac ventricular cells. Br J Pharmacol 119:555–563.

Yan YP, Dempsey RJ, Sun D (2001) Expression of Na^+-K^+-Cl^- cotransporter in rat brain during development and its localization in mature astrocytes. Brain Res 911:43–55.